CO4-1 Characterization of Additive Aggregation in Lubricant using Small-Angle X-ray Scattering

Y. Oba, M. Hino[1], R. Motokawa, N. Adachi[2], Y. Todaka[2], R. Inoue[1], and M. Sugiyama[1]

Materials Sciences Research Center, Japan Atomic Energy Agency
[1]Institute for Integrated Radiation and Nuclear Science, Kyoto University
[2]Department of Mechanical Engineering, Graduate School of Engineering, Toyohashi University of Technology

INTRODUCTION: In lubricants, nanostructures of additives are closely related to their lubrication properties. Although small-angle scattering is a promising means to characterize such nanostructures [1,2], it is not commonly used in the field of tribology. While small-angle neutron scattering (SANS) has been conducted in those previous studies, we have recently examined the application of small-angle X-ray scattering (SAXS) to the characterization of the additives in the lubricants [3]. The results show that SAXS is useful for the observation of the additives. While SANS can precisely analyze the nanostructures using contrast matching and variation techniques with deuterated samples, SAXS can provide easy access to experiments. However, a part of samples shows very weak scattering. Therefore, in this study, denser samples are measured to discuss the detail of the nanostructures of the additives.

EXPERIMENTS: SAXS measurements were performed using the in-house SAXS instrument with Mo *K*α radiation. Scattering patterns were obtained using a two-dimensional detector (PILATUS 100k) equipped with a 1000 μm-thick silicon sensor. The path of X-ray between the entrance slit and up to the detector including the sample area was in vacuum to eliminate background scattering from air and vacuum windows. Oleic acid (OA) and oleyl acid phosphate (OLAP) were chosen as the additive and poly-α-olefin (PAO) as base oil. In our previous study, we measured 5 mass% OA and 1 mass% OLAP dispersed in PAO [3]. In the current study, 20 mass% OA and 10 mass% OLAP in PAO were measured. The samples were sealed in sample cells with the optical path length of 10 mm. Two samples-to-detector distances (SDD), 0.4 and 1.8 m, were used to cover wide q range, where q is the magnitude of the scattering vector. The measurement times are 1 hour and 5 hours for 0.4 m and 1.8 m conditions, respectively.

RESULTS: Fig. 1 shows the SAXS profiles of 20 mass% OA in PAO, 10 mass% OLAP in PAO, and pure PAO. Based on our previous report [3], a peak at around q = 4.5 nm^{-1} reflects the nanostructures in PAO. Both OA and OLAP show additional scattering compared to PAO. Therefore, we successfully observe the nanostructures of these additives using SAXS. Compared to our previous

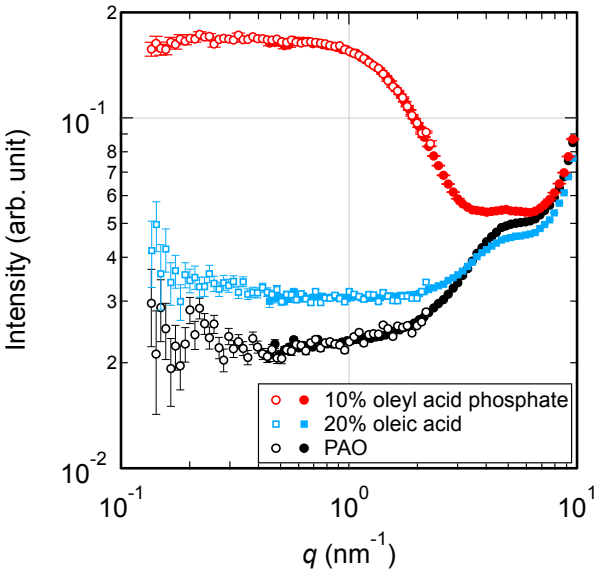

Fig. 1. SAXS profiles of 20 mass% OA in PAO, 10 mass% OLAP in PAO, and pure PAO. Open and filled symbols indicate the profiles obtained using SDD = 1.8 and 0.4 m, respectively.

study, OA indicates significant scattering. This is attributed to the denser concentration of 20 mass%. In the q range higher than 3.4 nm^{-1}, the scattering intensity of PAO exceeds that of 20 mass OA in PAO. This is probably due to the partial specific volume of OA.
Fig. 1 also shows that the SAXS profile of 10 mass% OLAP has a significant shoulder in the q range lower than about 2.5 nm^{-1}. This feature corresponds to the gyration radius of about 0.7–0.8 nm and larger than the size of a single OLAP molecule [4]. Hence, OLAP probably forms aggregate in PAO.
These result will promote further development of advanced lubricants in conjunction with the nanostructural characterization by SAXS.

ACKNOWLEDGMENTS: A part of this work was supported by JST "Collaborative Research Based on Industrial Demand" Grand Number JPMJSK1511, Japan.

REFERENCES:
[1] M. J. Covitch *et al.*, Adv. Chem. Eng. Sci., **5** (2015) 134-151.
[2] M. T. Savoji *et al.*, Ind. Eng. Chem. Res., **57** (2018) 1840-1850.
[3] Y. Oba *et al.*, KURNS Progress report 2019, (2020) 148.
[4] Y. Oba *et al.*, Chem. Lett. **49**, (2020) 823.

CO4-2 Radiation Tolerance of SiC p+n Junction-Diodes for Beam Monitor Applications

T. Kishishita, M. Hagiwara[1], M. M. Tanaka, H. Yashima[2], R. Kosugi[3]

High Energy Accelerator Research Organization, KEK
[1] National Institutes for Quantum Science and Technology
[2] Institute for Integrated Radiation and Nuclear Science, Kyoto University
[3] National Institute of Advanced Industrial Science and Technology

INTRODUCTION: Silicon carbide (SiC) has been considered as a potential alternative to Si for the manufacture of dosimeters, spectrometers, and charge particle detectors in high energy physics experiments, by virtue of its operation capability in strong radiation and/or high-temperature environments. To take advantage of such properties for future radiation detectors with a comparable size of silicon, we firstly investigated the influence of the bulk defects on the radiation sensor characteristics, by irradiating neutrons at Institute for Integrated Radiation and Nuclear Science, Kyoto University.

EXPERIMENTS: The reverse blocking characteristics is a primary concern of the radiation effects. The radiation-induced effects are generally divided into bulk and surface defects. The formers are caused by the displacement of crystal atoms, introducing to the increase of the leakage current and degraded reverse blocking characteristics. The latter include all effects in the covering dielectrics and the interface region. Since the bulk damage caused by the elastic nuclear scattering of the lattice nuclei has a profound effect in our device, we irradiated neutrons to pixelized diodes under unbiased conditions. The irradiation test was conducted by putting the samples at the Kyoto University nuclear reactor core. After disassembling of the samples, we carried out measurements of the leakage current and compared with those of the pre-irradiation samples.

RESULTS: The typical I-V characteristics before irradiation are shown in Figure 1. The leakage current shows a device-to-device dependence and are distributed between 1~8 nA at a reverse bias of 1 kV (corresponding to leakage current density of 10~83 nA/cm^2). The fundamental reason of the distribution is beyond comprehension, however, the bulk defects in the crystal are the natural interpretation. Figure 2 shows the typical leakage currents after irradiation. Compared with Fig. 1, the bulk leakage current in reverse bias is not increased after neutron irradiation of 1.63 x 10^{13} n_{eq}/cm^2 fluence, except the pixel-to-pixel dependence and data fluctuation due to the different sampling time settings. The reverse blocking property was also retained up to 3 kV. Irradiation tests at higher fluences are severe with the current device structure due to the radioactivation of the metals. We note that the 1 MeV neutrons have the same efficiency in the detector degradation as 24 GeV protons at a comparable neutron equivalent fluence. The theoretical nonionizing energy loss (NIEL) calculation performed on SiC can be found in Lee et al. [1]. The primary radiation defects produced by single particles (protons and pions) or gamma-rays were not evaluated in this measurement, however, the number of primary defects is reported as low as that of diamond. Thus, we conclude that the bulk defects introduced by irradiation at the 10^{13} neutron equivalent fluence is ignorable, in agreement with the previous studies on neutron-irradiated pn devices [2, 3].

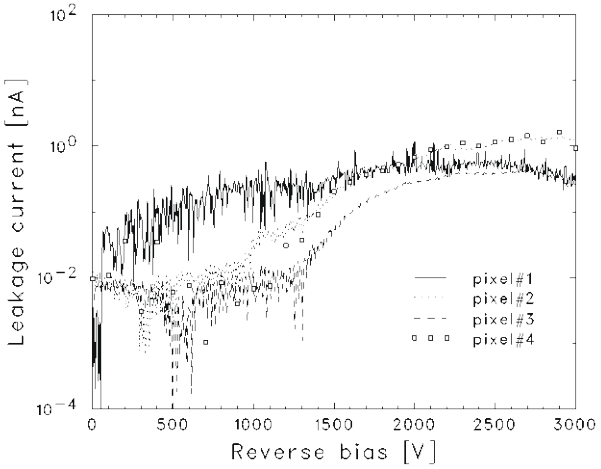

Fig. 1. Typical reverse blocking characteristics of the fabricated pixel diodes.

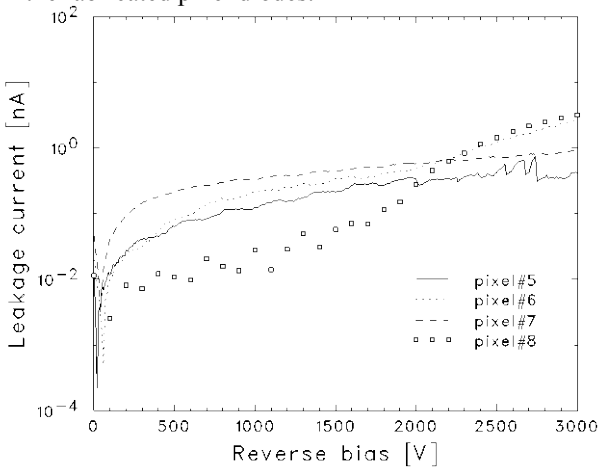

Fig. 2. Typical reverse blocking characteristics after 1 MeV neutron irradiation of 1.63 x 10^{13} n_{eq}/cm^2.

REFERENCES:

[1] K. K. Lee *et al*., Nucl. Instrum. Methods Phys. Res. B, vol.210, pp.489-494, 2003.
[2] F. Moscatelli *et al*., IEEE Trans. Nucl. Sci., vol.53, pp.1557--1563, 2006.
[3] J. M. Rafi *et al*, IEEE Trans. Nucl. Sci., vol.67, pp.2481--2489, 2020.

CO4-3 TDPAC Spectra of the ^{111}Cd(←^{111m}Cd) and ^{117}In(←^{117}Cd) Probes in $CdIn_2O_4$

W. Sato, S. Komatsuda[1], A. Taniguchi[2], M. Tanigaki[2], and Y. Ohkubo[2]

Institute of Science and Engineering, Kanazawa University
[1]Institute of Human and Social Sciences, Kanazawa University
[2]Institute for Integrated Radiation and Nuclear Science, Kyoto University

INTRODUCTION: Ternary spinel oxides exhibit various physical properties depending on the constituent metal elements and on their distribution between the tetrahedral *A* site and octahedral *B* site. Among various metal elements, it is known that Cd^{2+} is likely to occupy the *A* site forming normal spinel with divalent ions and trivalent ions on the *A* and *B* sites, respectively. In our recent time-differential perturbed angular correlation (TDPAC) experiments on Cd spinel compounds such as $CdFe_2O_4$ and $CdIn_2O_4$, we noticed unexpected phenomenon that the directional anisotropy of the cascade γ rays emitted from the ^{111}Cd(←^{111m}Cd) probe shows exponential-like relaxation as if the nuclear spin would experience dynamic perturbation from the extranuclear field [1,2]. If the attenuation of the anisotropy arises from dynamic perturbation, we can expect temperature dependence of the relaxation constant λ as in the following expression of the time-differential perturbation factor $G_{22}(t)$ as a function of the time interval t between the cascade γ-ray emission:

$$G_{22}(t) = \exp(-\lambda t). \qquad (1)$$

In order to provide insight into the phenomenon, we have obtained high temperature TDPAC spectra for $CdIn_2O_4$, using two different probes ^{111}Cd(←^{111m}Cd) and ^{117}In(←^{117}Cd). Here, a preliminary result is reported.

EXPERIMENTS: Neutron irradiation was performed for cadmium oxide (CdO) enriched with ^{110}Cd and ^{116}Cd in Kyoto University Reactor to produce radioactive ^{111m}Cd and ^{117}Cd, respectively, by neutron capture reactions. Each of the radioactive Cd(^{111m}Cd)O and Cd(^{117}Cd)O powders was separately mixed well with stoichiometric amounts of CdO and In_2O_3 in an agate mortar. The mixtures were then pressed into disks and sintered in air at 1373 K for 45 min.
TDPAC measurements were carried out for the ^{111}Cd(←^{111m}Cd) and ^{117}In(←^{117}Cd) probes with the intermediate states of I = 5/2 and 3/2 having half-lives of 85.0 and 54.6 ns, respectively. In the present work, we obtained the perturbed angular correlation as a function of the time interval of the cascade γ-ray emissions by the following expression:

$$A_{22}G_{22}(t) = \frac{2[N(\pi,t) - N(\pi/2,t)]}{N(\pi,t) + 2N(\pi/2,t)}, \qquad (2)$$

where A_{22} denotes the angular correlation coefficient and $N(\theta, t)$ stands for the number of the delayed coincidence events observed at an angle θ. The measurements were performed at 973 K.

RESULTS: The TDPAC spectra of ^{111}Cd(←^{111m}Cd) and ^{117}In(←^{117}Cd) in $CdIn_2O_4$ are shown in Fig. 1. The spectrum of ^{111}Cd(←^{111m}Cd) (Fig. 1(a)) exhibits a relaxing trend in the directional anisotropy, which is similar to the spectra observed at room temperature and 77 K [1]. However, the relaxation time seems a little longer for the present spectrum. This slight temperature dependence may suggest that the motion of charges surrounding the probe is thermally activated at the present high temperature. The spectrum of ^{117}In(←^{117}Cd) also shows gradual attenuation of the directional anisotropy. It should be noted that the probe nuclei having interaction with the extranuclear fields are of different elements, Cd and In. Thus, the present observation demonstrates that the probes of different elements are perturbed in the same way and show similar spectral patterns. In order to clarify the cause of the spectral attenuation, detailed temperature dependence needs to be investigated.

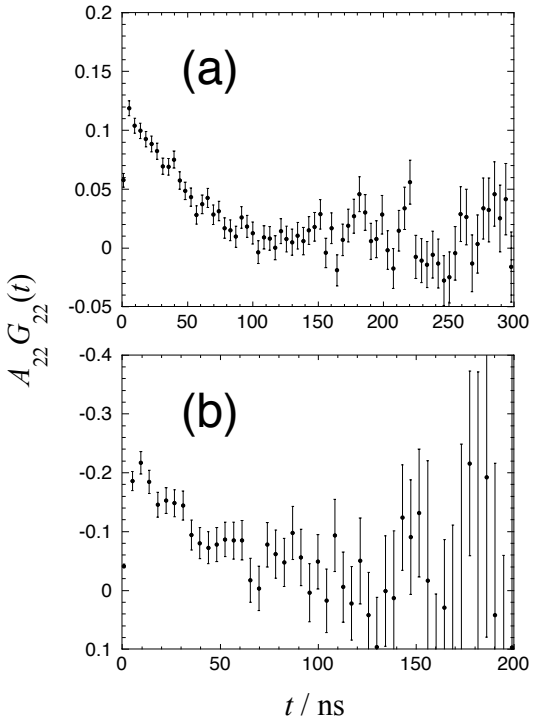

Fig. 1. TDPAC spectra (a) of ^{111}Cd(←^{111m}Cd) and (b) of ^{117}In(←^{117}Cd) in $CdIn_2O_4$ measured at 973 K.

REFERENCES:

[1] W. Sato *et al.*, J. Radioanal. Nucl. Chem., **316** (2018) 1289-1293.
[2] W. Sato *et al.*, KURNS Prog. Rep., **2020** (2021) 113.

CO4-4 Synthesis of metal nanocomplexes in water solution by γ-ray and electron irradiation reduction

F. Hori, K. Zhu, T. Yamada, T. Matsui[1], N. Taguchi[2], S. Tanaka[2] and Q. Xu[3]

Dept. of Engineering, Osaka Prefecture University

[1]*Center for Advanced Education of Entrepreneurship and Innovation, Osaka Prefecture University*

[2]*AIST, Kansai Center*

[3]*KURNS*

INTRODUCTION: It is known that metal nanoparticles (NPs) have some specific properties, which are not appeared in bulk materials such as catalytic activities, magnetic properties, electric conductivity and light absorption. These properties depend on its size, shape, structure, chemical composition and so on. In general, metal nanoparticles can be produced by various top-down and bottom-up methods. Above all, chemically synthesizing as bottom-up method can control the size and shape of it. However, it is not easy to fabricate multi elemental alloy NPs controlling with their structure. Almost fabrication method of NPs with commercially is based on equilibrium chemical reaction in ionic solution with reduction additive. We have been studying to synthesize various metal NPs by non-equilibrium reaction method that is reduction reactions induced by ultrasonic, solution plasma, electron beam, ion beam and gamma-ray irradiation into aqueous solution [1]. Recently, by using this radiation reduction method, we have been trying to synthesize metal nanocomposites. In this study, we have studied the fine structure of nanoparticles synthesized by electron and gamma-ray irradiation reduction in water solutions including multiple metal ions.

EXPERIMENTS:

Aqueous solutions with various ternary combination of a given concentration of metal complexes ($(CH_3COO)_2Cu{\cdot}H_2O$), $AgNO_3$, NiCl, $Na[AuCl_4]$ and $PdCl_2NaCl_3H_2O$ with an additive of polyvinyl (PVP) and 8.5 vol% ethylene glycol were prepared. The ratio of all ions concentration was adjusted to the ratio of 0.5 to 2.0 in the solution. The solution was argon gas purged and sealed into polystyrene vessels. They were irradiated at about 300 K with 1.17 and 1.33 MeV gamma-rays from ^{60}Co radio active source at gamma irradiation facility in KURRI, Kyoto University. The total dose was fixed to 10 kGy with the dose rate of 1.0 kGy/h. Also, same solutions were irradiated 8 MeV electron with total dose of 10kGy in about 60 sec by linear accelerator at same facility. After irradiation, the samples were measured for UV–vis absorption spectra. The structures for all colloidal products were examined by X-ray absorption fine structure (EXAFS) and X-ray photoelectron spectroscopy (XPS) at KEK-PF BL-27, X-ray diffraction and transmission electron microscope.

RESULTS:

Fig. 1 shows the TEM image of nanoparticles synthesized by electron and gamma-ray irradiation reduction methods in the solution including Ag, Au, Cu and Ni ions. As is seen in these figures, the size of nanoparticles are cleary different. This is because the higher reduction rate of electron irradiation than that of gamma-ray irradiation. This result is in good agreement with the result of correlation of particle size produced by irradiation with different irradiation reduction rates [2].

Fig. 2 shows the EXAFS spectra of synthesized nanoparticles in a AgAuCu ternary solution after electron and gamma-ray irradiation reduction. In case of electron irradiation, only one peak appeared but double peaks appeared in case of gamma-ray irradiation. These peaks originated from Cu-O and Cu-Cu metal combinations mainly. It found that the main products are Cu-oxide in case of electron irradiation, and Cu-metal alloy nanocomposites in case of gamma-ray irradiation.

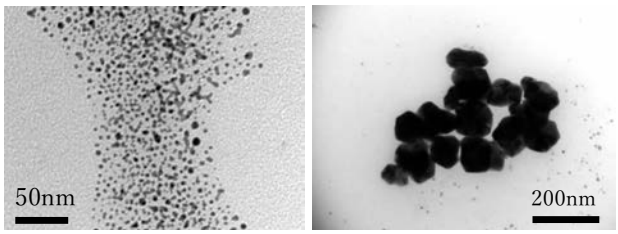

Fig.1. TEM images of products in a Ag, Au and Cu ions solution synthesized by (a) electron irradiation and (b) gamma-ray irradiation.

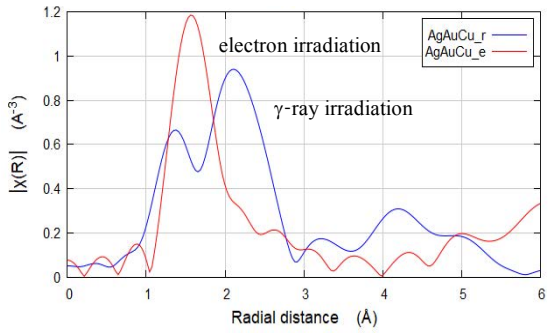

Fig. 2 EXAFS spectra of electron and gamma-ray irradiation reduction solutions including Ag, Au and Cu Au ions.

REFERENCE:

[1] N. Taguchi *et al.*, Rad. Phys. Chem. 78, (2009) 1049-1053.
[2] N. Maeda *et al.*, Mater. Res. Soc. Symp. Proc. Vol. 900E.

CO4-5 Hydrogen trapping behavior at vacancy in Fe-Al alloy with electron irradiation

F. Hori, H. Otomo, H. Obayashi, Y. Morikuni, K. Ohsawa[1], Q. Xu[2], N. Abe[2], A. Iwase[3] and K. Yasunaga[3]

Dept. of Quantum & Radiation Eng., Osaka Pref. Univ.
[1]*Res. Inst. of Appl. Mech., Kyushu University*
[2]*KURNS*
[3]*Wakasa-wan Energy Research Center*

INTRODUCTION: Intermetallic compounds have good properties such as specific strength to weight ratio, oxidation resistance and strength in elevated temperature. In addition, some of them can be applied for hydrogen storage material by production of hydride such as Mg and Ni based compound alloys. On the other hand, it found that hydrogen absorption properties in some compound alloys. It is reported that novel Ni- based alloy including defect type free volume can be used as hydrogen permeation membranes to separate H_2 from CO_2 and other gases obtained from water. Also, first principle calculation result shows that not only one hydrogen atom but some number of hydrogen atoms possibly be trapped by a single vacancy in B2 ordered Fe-Al alloy. However, the interaction between vacancy and hydrogen atom in this type of Fe-Al alloy is not cleared yet. So far, we have been studied defects behavior introduced by various energetic electron and ions irradiation. In this study, we have studied the interaction between hydrogen atom and non-equilibrium vacancies introduced by electron irradiation.

EXPERIMENTS: B2 ordered Fe-Al alloys were prepared by arc melting method in argon gas atmosphere. Sliced samples with the thickness of 0.5 mm were annealed at 1273 K for 20 h and cool down to 973 K slowly and then quenched into water. These specimens were irradiated with 8 MeV electron up to the fluence of 4×10^{18} /cm^2 at KURRI, Kyoto University. Irradiation was carried out at about 330 K with temperature controlling water cool system. Hydrogen was introduced for unirradiated and electron irradiated samples at 0.1 mA/cm^2 in a NH_4SCN solution bath added 0.001 mol/L H_2SO_4 by electro chemical method for 8 hours. These samples were examined by X-ray diffraction (XRD). Also, the thermal desorption spectroscopy (TDS) was measured with heating rate of 1 K/s.

RESULTS: Figure 1 shows the X-ray diffraction spectra of Fe-Al alloy before, after electron irradiation and hydrogen charged after irradiation. The movement of the Bragg peak of (211) plane to a slightly higher angle is considered to be due to the formation of point defects by electron irradiation. But this peak shift recovered after hydrogen introduction. This is considered to be due to hydrogen trapping at vacancy site. Figure 2 shows the TDS spectra for hydrogen introduced Fe-Al alloys with and without electron irradiation. This figure clearly shows that the amount of absorbed hydrogen after electron irradiation is larger than that without irradiation. In addition, a sharp peak appears at 650 K, which indicates the dissociation temperature of hydrogen atoms from the pores introduced by electron irradiation.

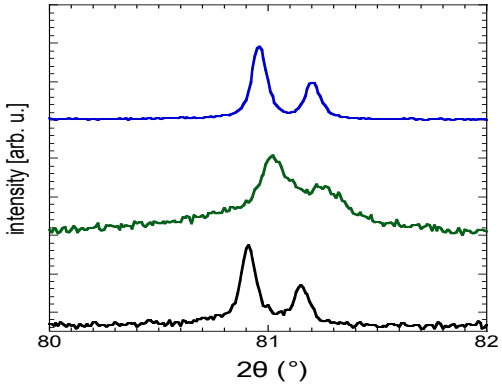

Fig. 1 XRD profiles of Fe-Al alloy before irradiation, after electron irradiation and hydrogen introduced after irradiation.

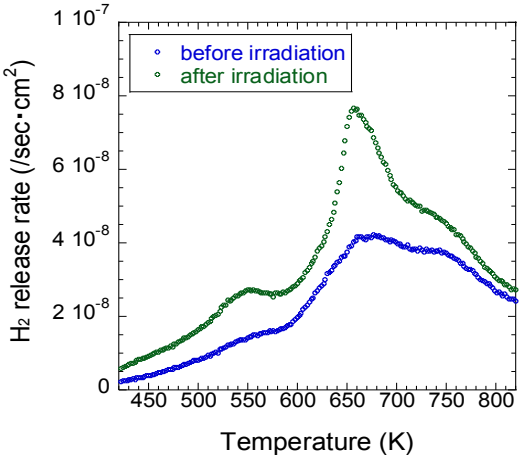

Fig. 2 TDS spectrum of hydrogen introduced into electron-irradiated and unirradiated Fe-Al alloy samples.

CO4-6 Study of resonant frequency change with irradiation dose of piezoelectric PZT element

M. Kobayashi, T. Miyachi, S. Takechi[1], Reo Kunimatsu[1], Ryo Sasaki[1], Masaya Danjohbara[1] and Haruki Oh'ishi[1]

Planetary Exploration Research Center, Chiba Institute of Technology
[1]Graduate School of Engineering, Osaka City University

INTRODUCTION: This study aims to establish an inexpensive method for dosimetry in high-dose environments. We consider changes in piezoelectric properties of piezoelectric elements due to irradiation for dosimetry in high-dose environments. For this purpose, the mechanism of radiation-induced change of piezoelectric properties has been investigated.

In a previous experiment conducted at NIRS/HIMAC, piezoelectric PZT elements were irradiated with 400 MeV/n Xe particles, and the decrease in the electromechanical coupling coefficient k was investigated [1]. As a result, it was found that k_r of the irradiated PZT element was -0.35%/kJ, which is a phenomenon concerning the irradiation dose. In order to investigate what happens to piezoelectric elements due to irradiation, electron beam irradiation experiments have been conducted at KUR/LINAC. The effect of temperature, which was negligible in the Xe particle experiments, has been investigated and controlled in the experiments at KUR/LINAC.

EXPERIMENTS IN THE FISCAL YEAR 2021: The geometry of the PZT element that has been irradiated so far was changed from a cylindrical shape of ϕ 18 mm x t12 mm to a disk shape of ϕ 18 mm x t1 mm. This shape satisfies the conditions of the approximate formula for determining k, and the evaluation of k value as an absolute value can now be performed instead of the evaluation of relative changes. Furthermore, the thickness of the electron-beam irradiation target was made thinner, which reduced the number of neutrons produced and thus met the objective of this experiment, which was to investigate the contribution of electron beams alone. The thinner target also improves the air-cooling effect during irradiation, and the temperature can be suppressed to a moderate value (≤90°C) even with an electron dose of 4.8 μA, whereas the irradiation current is about 1 μA for the conventional device, thus shortening the irradiation time from half a day to about one hour. This enabled us to shorten the irradiation time from half a day to about one hour, thereby improving the efficiency of the experiment.

In addition to such experimental setup, experiments were conducted to investigate the difference in response to electron irradiation between different types of PZT elements (soft PZT, high-temperature soft PZT, and high-temperature hard PZT), which are the specimens. The difference between the "soft" and "hard" materials is simply that the "soft" material is more or less distorted when a voltage is applied to it. The "high-temperature" materials are those that have a high Curie temperature at which they are completely depolarized. Table 1 summarizes the percentage change in k after electron irradiation of each PZT. This is a summary of the experimental results using four samples for the soft material, three samples for the high-temperature soft material, and three samples for the high-temperature hard material. The k_t in the thickness direction of the high-temperature soft material is not shown due to measurement problems.

DISCUSSION: The mechanism of radiation-induced degradation on piezoelectric PZT element was discussed. However, the effect of depolarization caused by temperature rise due to irradiation is excluded. Radiation-induced degradation includes (1) migration of atoms in crystals, (2) conversion to other nuclides by nuclear reactions, (3) acceleration of chemical reactions such as cross-linking or oxidation (mainly in polymer materials), and (4) dielectric breakdown due to charge accumulation generated by ionizing effects (mainly in semiconductors). The change in the properties of PZT due to electron irradiation is considered to be dominated by (4). Analysis of gamma-ray spectra immediately after irradiation shows that the number of activated atoms is limited. It is noteworthy that k is larger in the high-temperature hard material. At first glance, this appears to be an increase in piezoelectricity, but it may be that the destruction of the domain walls inside the piezoelectric ceramics "softens" the entire element and increases electromechanical coupling coefficient k. In this case, the domain walls would be ionized by radiation. In this case, the domain walls may have been destroyed by the electric charge accumulated by ionization due to radiation. We would like to investigate this further in the future.

Table 1. Variation rate of coupling coefficient k per unit absorbed dose.

PZT type	Δk_r[%/kJ]	Δk_t[%/kJ]
Soft	−0.090 ± 0.013	−0.10 ± 0.059
High temp. soft	−0.087 ±0.038	---
High temp. hard	+0.13 ± 0.081	−0.050 ± 0.0061

REFERENCES:

[1] S. Takechi *et al.*, Japanese Journal of Applied Physics 60 038003 (2021).
[2] M. Kobayashi *et al.*, Japanese Journal of Applied Physics 53, 066602 (2014).
[3] M. Kobayashi *et al.*, Japanese Journal of Applied Physics 52, 126604 (2013).

CO4-7 Concentration Dependence of Local Structures at Cd Sites in $Cd_xSr_{1-x}TiO_3$ Studied by TDPAC Method

S. Komatsuda, W. Sato[1], A. Taniguchi[2], M. Tanigaki[2], and Y. Ohkubo[2]

Institute of Human and Social Sciences, Kanazawa University
[1]*Institute of Science and Engineering, Kanazawa University*
[2]*Institute for Integrated Radiation and Nuclear Science, Kyoto University*

INTRODUCTION: Strontium titanate ($SrTiO_3$) is a cubic perovskite compound of ABO_3 type. Among ABO_3 perovskites, $SrTiO_3$ has a wide band gap values of 3.2 eV, and doping effect of $SrTiO_3$-based materials is attracting much attention. It is known from many previous reports that chemical and physical properties of $SrTiO_3$ change depending on the kind of dopant ions and the surrounding local structures[1]. For a practical use of $SrTiO_3$, it is necessary to obtain more microscopic information on various impurity sites. Therefore, we applied the time-differential perturbed angular correlation (TDPAC) method to study the local structures at impurity sites in $SrTiO_3$. In our previous TDPAC study of $SrTiO_3$ doped with the ^{111}Cd($\leftarrow{}^{111}$In) probe, it is suggested that In dopants replace Sr^{2+} and Ti^{4+} in the lattice sites where defect exists in the vicinity of the probes. In order to obtain further information on the local fields at various impurity sites, we have thus performed TDPAC measurements for $SrTiO_3$ with ^{111}Cd($\leftarrow{}^{111m}$Cd) probe, the same probe, but descended from a different parent nucleus. In order to uniformly introduce ^{111}Cd($\leftarrow{}^{111m}$Cd) probe in $SrTiO_3$, we first studied local structure of the ^{111}Cd($\leftarrow{}^{111m}$Cd) in $Cd_xSr_{1-x}TiO_3$ at various Cd concentration. We here report part of the result of TDPAC measurements for the ^{111}Cd($\leftarrow{}^{111m}$Cd) in $Cd_xSr_{1-x}TiO_3$

EXPERIMENTS: Stoichiometric amount of $SrCO_3$, $CdCO_3$, and TiO_2 powders were mixed in the mortar. The powders were pressed into disks. For TDPAC measurements, about 3 mg of CdO enriched with ^{110}Cd was irradiated with thermal neutrons in Kyoto University Research Reactor, and radioactive ^{111m}Cd was generated by ^{110}Cd(n, γ)^{111m}Cd reaction. The neutron-irradiated CdO powder was dissolved in 6M HCl and added in droplets onto the pre-sintered $Cd_xSr_{1-x}TiO_3$ disk. The disk was sintered in air at 1373 K for 90 min. The TDPAC measurement was carried out for the 151-245 keV cascade γ rays of ^{111}Cd($\leftarrow{}^{111m}$Cd) probe with the intermediate state of I = 5/2 having a half-life of 85.0 ns.

RESULTS: Figure 1 shows the TDPAC spectra of ^{111}Cd($\leftarrow{}^{111m}$Cd) (a) in $Cd_xSr_{1-x}TiO_3$ (x = 0.04) and (b) in $Cd_xSr_{1-x}TiO_3$ (x = 0.06) at room temperature. The directional anisotropy on the ordinate, $A_{22}G_{22}(t)$, was deduced with the following simple operation for delayed coincidence events of the cascade:

$$A_{22}G_{22}(t)=\frac{2[N(\pi,t)-N(\pi/2,t)]}{N(\pi,t)+2N(\pi/2,t)}. \qquad (1)$$

Here, A_{22} denotes the angular correlation coefficient, $G_{22}(t)$ the time-differential perturbation factor as a function of the time interval, t, between the relevant cascade γ-ray emissions, and $N(\theta,t)$ the number of the coincidence events observed at angle, θ. With respect to Fig. 1(a), the spectral pattern is damped. Because the dynamic perturbation should not be considered in a TDPAC measurement at room temperature, the spectral pattern was fitted with two static electric quadrupole frequencies which have large distribution widths (δ = 27(7)%, 82(12)%). These large values of distribution widths indicate local randomness at ^{111}Cd($\leftarrow{}^{111m}$Cd) probe sites in $Cd_xSr_{1-x}TiO_3$. On the other hand, the spectrum in Fig. 1(b) can be reproduced by a fit with three unique quadrupole frequencies, which suggests that ^{111}Cd($\leftarrow{}^{111m}$Cd) probes occupied three specific lattice sites in $Cd_xSr_{1-x}TiO_3$. These experimental results show that Cd ions dispersed into $Cd_xSr_{1-x}TiO_3$ perovskite structure at atomic scale by increase of Cd ratio from x = 0.04 to x = 0.06. This concentration dependence of local structure at Cd site might be attributed to the change of lattice constant of $Cd_xSr_{1-x}TiO_3$. For more information on this concentration dependence, investigations of lattice constants of $Cd_xSr_{1-x}TiO_3$ perovskite are now in progress.

REFERENCE:

[1] C. M. Culbertson *et al*., *Scientific Reports* **10** (2020) (3729(1)-3729(10)).

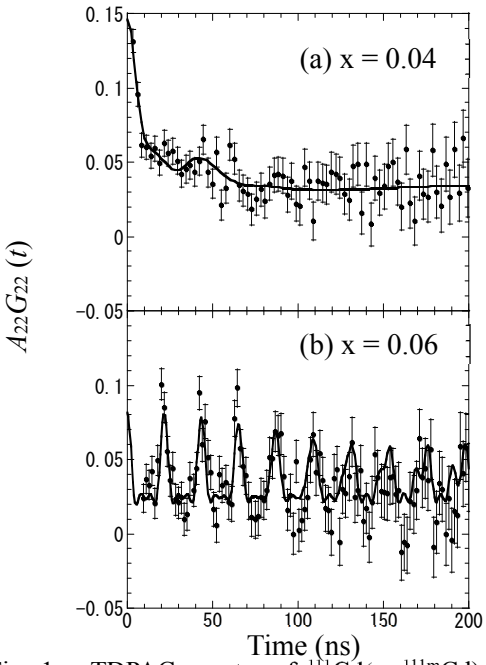

Fig. 1. TDPAC spectra of ^{111}Cd($\leftarrow{}^{111m}$Cd) (a) in $Cd_xSr_{1-x}TiO_3$ (x = 0.04) and (b) in $Cd_xSr_{1-x}TiO_3$ (x = 0.06) at room temperature.

CO4-8 Operation of Field Emission Image Sensor under Gamma-ray Irradiation

Y. Gotoh, Y. Neo[1], K. L. Zheng[1], M. Nagao[2], T. Okamoto[3], N. Sato[4]

Graduate School of Engineering, Kyoto University
[1]Instittute of Electronics, Shizuoka University
[2]National Institute of Advanced Industrial Science and Technology
[3]National Institute of Technology, Kisarazu College
[4]Institute for Integrated Radiation and Nuclear Science, Kyoto University

INTRODUCTION: In decommissioning of Fukushima Daiichi Nuclear Power Plant, radiation tolerant image sensors are strongly demanded. We have been developing a vacuum-based image sensor, which is consisted of a matrix type field emitter array (FEA), a mesh electrode and a photoconductor film (field emission image sensor) [1]. The image sensor detected light signal even after the gamma-ray irradiation to the dose of 1 MGy. Operation of field emitters under gamma-ray irradiation was demonstrated and no significant change of the properties due to gamma-ray irradiation could not be detected [2]. However, imaging characteristics under gamma-ray irradiation has not yet been confirmed. In this study, variation of the photo-signal detection properties with and without gamma-ray irradiation was investigated.

EXPERIMENTS: The FEA used in the present study was fabricated at National Institute of Advanced Industrial Science and Technology [3], and possessed 1,024 hafnium carbide emitters. It should be stressed here that the FEA was not a matrix-type. Cadmium telluride/cadmium sulfide photo diode, which was originally developed as a solar cell was used as an anode (photoconductor) [4]. Antimony sulfide thin film was formed on the surface of the photoconductor. The FEA, mesh electrode and anode were installed in a vacuum vessel which was evacuated by a non-evaporable getter pump. Gamma-ray irradiation was performed at Cobalt-60 Gamma-ray Irradiation Facility, Institute for Integrated Radiation and Nuclear Science, Kyoto University. The vacuum vessel was settled in the irradiation room at the position 30 cm away from the gamma-ray source. An electric light was also settled in the irradiation room to illuminate the image sensor. The emitter was grounded and the gate was positively biased to extract the electrons. The mesh and the anode were also positively biased, typically 120 V and 10 V, respectively. After several measurements of anode current-gate voltage characteristics, operation of the image sensor was conducted. Giving a fixed voltage to the gate, the variation of the anode current was observed with and without light illumination under gamma-ray irradiation.

RESULTS: Figure 1 shows the variation of the anode current under gamma-ray irradiation. The estimated dose rate of irradiation was about 220 Gy h^{-1}, which is higher than that of irradiation observed in the primary containment vessel of Fukushima Daiichi Nuclear Power Plant [5]. The electric light was turned on and off every 10 seconds to confirm the capability of photo-signal detection. As is shown in Fig. 1, the anode current showed a step like variation, of which interval corresponded to the interval of the light illumination. From this figure, it is shown that the present device could detect photo-signal even under high dose rate gamma-ray irradiation. The intensity of illumination could not be evaluated in this study, so measurements with known intensity of illumination is necessary to estimate the property of the image sensor. Small signal would be attributed to the poor adjustment of the operating conditions of the image sensor. Deterioration of the antimony sulfide layer would be another reason. The device configuration was not fully optimized in the present study. Therefore, improvement of the device performance can be expected, optimizing the operating condition and device configuration.

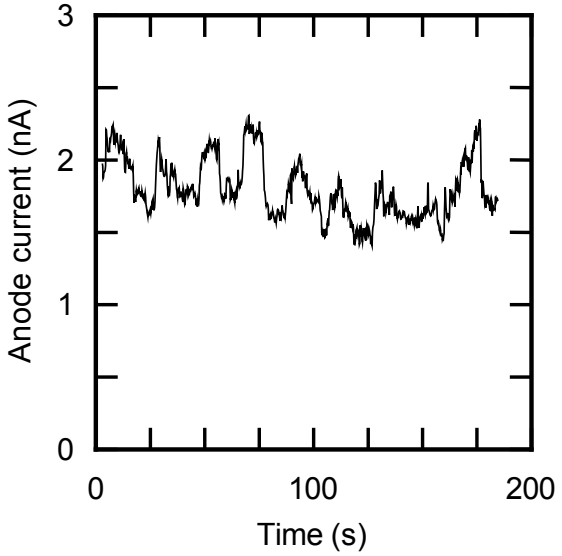

Figure 1. Variation of the anode current with and without light illumination under the gamma-ray irradiation.

REFERENCES:

[1] Y. Gotoh *et al.*, IEEE Trans. ED **67** (2020) 1660-1665.
[2] Y. Gotoh *et al.*, KURRI Progress Report 2018 (2018) CO4-3.
[3] T. Sato *et al.*, J. Vac. Sci. Technol. B **21** (2003) 1589-1593.
[4] T. Okamoto *et al.*, Jpn. J. Appl. Phys. **60** (2021) SBBF02.
[5] Fukushima Daiichi Nuclear Power Plant, Investigation Results Inside Unit 2 PCV. Accessed: April 22, 2022. [Online]. Available: https://www.meti.go.jp/earthquake/nuclear/decommissioning/committee/osensuitaisakuteam/2019/02/3-3-3.pdf.

CO4-9 Radiochemical Research for the Advancement of $^{99}Mo/^{99m}Tc$ Generator by (n, γ) Method (4)

Y. Fujita, M. Seki, M. C. Ngo[1], T. M. D. Do[1], X. Hu[1], Y. Yang[1], T. Takeuchi, H. Nakano, Y. Fujihara[2], H. Yoshinaga[2], K. Nishikata, T. Omori, J. Hori[2], T. Suzuki[1], H. Suematsu[1] and H. Ide

Department of JMTR, Japan Atomic Energy Agency
[1]Graduate School of Engineering, Nagaoka University of Technology
[2]Institute for Integrated Radiation and Nuclear Science, Kyoto University

INTRODUCTION: The research and development (R&D) has been carried out to produce Molybdenum-99 (^{99}Mo) by the neutron activation method ((n, γ) method) from viewpoints such as nuclear security. In order to apply the (n, γ) method to the $^{99}Mo/^{99m}Tc$ generator, it is necessary to improve the properties of Alumina (Al_2O_3) used as Mo adsorbent. To date, we have evaluated the quality of the ^{99m}Tc solution obtained from the column packed with the developed Al_2O_3 specimens. However, the problem was that ^{99}Mo was desorbed in the solution[1]. In this work, we evaluated the quality of the ^{99m}Tc solution obtained by taking measures to reduce the desorption of ^{99}Mo. The measures are (1) application of dynamic adsorption, (2) increasing the concentration of the sodium molybdate solution (Mo solution), (3) reducing the amount of Mo added, (4) acid treatment of the alumina specimens, and (5) sufficient washing of the alumina specimens.

EXPERIMENTS: MoO_3 pellet pieces irradiated with Pn-2 were dissolved with 6M-NaOHaq. The Mo concentration of the solution was adjusted to about 330 g/L, and the pH was adjusted to 2 - 3 by adding concentrated hydrochloric acid. Four types of alumina specimen (D-201-300, V-V-300, V-B-300, Medical Alumina)[2] were prepared and immersed in hydrochloric acid at pH3 overnight for acid treatment. A fluororesin column (ID 9 mm × 62 mm) whose shape was same as that built into a commercial $^{99}Mo/^{99m}Tc$ generator was filled with 2 g of each alumina specimen. The column was connected to a peristaltic pump and 0.2 mL of Mo solution was added to each column. Then, fifty milliliter of saline was flowed through the columns to wash thoroughly. After 24 hours, ten milliliter of saline was flowed through the columns to obtain ^{99m}Tc solutions as milking process. The eluate was collected as 1mL aliquots. The flow rate was approximately 40 mL/h. The milking was carried out for 2 days. The activities of obtained solution were measured by a gamma ray spectrometer.

RESULTS: The ^{99}Mo specific activity of the Mo solution was 13.1 MBq/g-Mo when the solution was added to the columns.
Table 1 shows the Mo adsorption capacities of each alumina specimen. The alumina specimens were subjected to acid treatment, but the adsorption capacities didn't improve. About 90% or more of ^{99m}Tc was eluted with 4 mL of saline with the developed alumina specimen.

Table 1. Mo adsorption capacities of alumina specimen.

	D-201-300	V-V-300	V-B-300	Medical Alumina
Mo adsorption capacity ($mg/g\text{-}Al_2O_3$)	24.1	31.4	30.8	28.8

On the other hand, ^{99}Mo was contained in the ^{99m}Tc solutions eluted from the columns. In the Minimum Requirements for Radiopharmaceuticals of Japan (MRRP), the desorbed ^{99}Mo amount in ^{99m}Tc solution is specified using the $^{99}Mo/^{99m}Tc$ ratio as an index. The standard value is $^{99}Mo/^{99m}Tc \leq 0.015\%$. Fig.1 shows a comparison of the $^{99}Mo/^{99m}Tc$ ratio of the ^{99m}Tc solution in the present work and the previous work. In the ^{99}Mo desorption reduction measures, the acid treatment of alumina had no effect. However, due to the application of dynamic adsorption, increasing the concentration of Mo solution, and reducing the amount of Mo added, the $^{99}Mo/^{99m}Tc$ ratio was significantly improved and reduced by about 50%. Therefore, it was suggested that the application of dynamic adsorption, increasing the concentration of Mo solution and reducing the amount of Mo added are effective in improving the Mo desorption property.

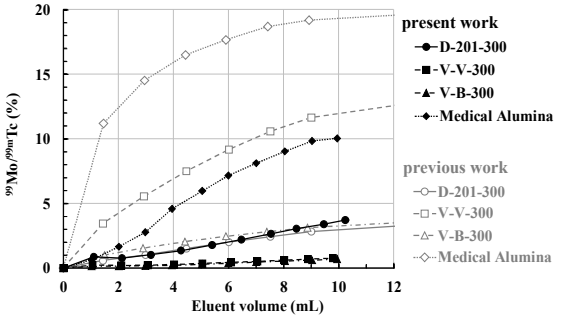

Fig. 1. Comparison of the $^{99}Mo/^{99m}Tc$ ratio of the ^{99m}Tc solution in the present work (dynamic adsorption) and the previous work (static adsorption) on day 1.

The pH standard value of the ^{99m}Tc solution is specified as pH 4.5 to 7.0. The pH of the ^{99m}Tc solution obtained from the developed alumina specimens deviated to the basic side.
In this work, the ^{99m}Tc solution didn't meet the MRRP, but it was suggested that the quality could be improved by changing the adsorption method and conditions. It is difficult to meet the MRRP with the current column shape. In the future, we will improve the quality of the ^{99m}Tc solution for practical use by optimizing the column shape and Mo adsorption conditions.

REFERENCES:

[1] Y. Fujita *et al.*, J. Radioanal. Nucl. Chem. **327**(2021) 1355-1363.
[2] Y. Suzuki *et al.*, Transactions of the Materials Research Society of Japan, **43**(2018)75-80.

CO4-10 The effect of ion irradiation on yttria stabilized zirconia (YSZ) single crystal substrates using a slow positron beam

T. Ozaki, H. Sakane[1], A. Yabuuchi[2] and A. Kinomura[2]

School of Engineering, Kwansei Gakuin University
[1] SHI-ATEX Co., Ltd.
[2] Institute for Integrated Radiation and Nuclear Science, Kyoto University

INTRODUCTION: The rare-earth (RE)-based cuprate superconductor $REBa_2Cu_3O_y$ (REBCO) exhibits high-temperature superconductivity and is expected to be useful for magnetic coils. Critical current properties in applied magnetic fields are improved by introducing lattice defects using ion-irradiation techniques. Positrons are sensitive to vacancy-type defects, and they are useful for characterizing irradiation-induced defects. However, it is difficult to characterize irradiation-induced defects in GdBCO coated conductors (CCs), which were industrially produced with a roll-to-roll process because GdBCO CCs initially contain vacancy clusters, whose size is larger than that of the newly-formed defects induced by the irradiation [1]. In this study, yttria stabilized zirconia (YSZ), which is an oxidized material and almost the same density as GdBCO, single crystal substrates were irradiated with He ions at 600 keV or Au ions at 10 MeV, and then probed using a slow positron beam.

EXPERIMENTS: The YSZ single crystal substrates were irradiated with 600 keV He^+ (< 2.0×10^{16} cm^{-2}) or 10 MeV Au^{4+} (< 7.0×10^{13} cm^{-2}) ions. The unirradiated and irradiated samples were probed by the KUR slow positron beam and the Doppler broadening of annihilation radiation (DBAR) spectra were acquired with incident positron energies E_+ = 9 keV. Figure 1 shows positron implantation profile. The sharpness of the DBAR spectra is evaluated by a value called the *S*-parameter, which becomes generally lower when positrons annihilate in a perfect lattice, and higher when positrons are trapped into vacancies [2].

RESULTS: Figure 2(a) and 2(b) show dose dependence of *S*-parameter for YSZ single crystals irradiated at 600 keV He^+ and 10 MeV Au^{4+} ions, respectively. *S*-parameter is closely correlated to concentration and size of defects in a material. As shown in Fig. 2, *S*-parameters increases with increasing fluence up to 1.0×10^{16} cm^{-2} for He-ion irradiation and 2.0×10^{13} cm^{-2} for Au-ion irradiation, above which no significant increase can be observed. This indicates that almost all of the positrons are trapped at irradiation-induced vacancy-type defects in the samples with the saturated *S*-parameter value. The saturated *S*-parameter value of YSZ single crystal substrate irradiated at 10 MeV Au ions is larger than that of the one irradiated at 600 keV He ions. This could be because the size of irradiation defect produced by Au-ions is larger than that of the one produced by He-ions.

REFERENCES:
[1] A. Yabuuchi *et al*., Appl. Phys. Express, 13 (2020) 123004.
[2] R. W. Siegel, Ann. Rev. Mater. Sci., 10 (1980) 393−425.

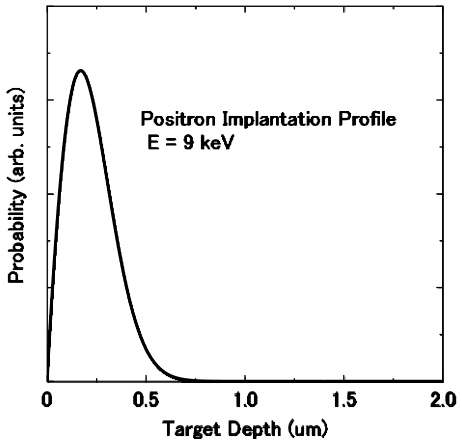

Fig. 1. Positron implantation profile in YSZ single crystal substrate.

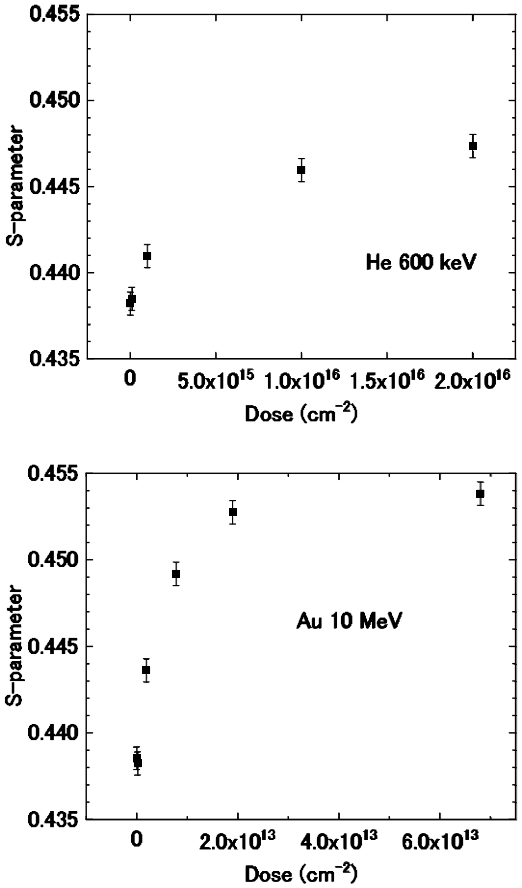

Fig. 2. Dose dependence of *S*-parameter for YSZ single crystals substrate irradiated at (a)600 keV He^+ and (b)10 MeV Au^{4+} ions.

CO4-11 Study on formation mechanisms of low-fluence ion-irradiation induced damages on semiconductor surfaces

J. Yanagisawa, R. Shigesada, Q. Xu[1], A. Yabuuchi[1], K. Takamiya[1], and A. Kinomura[1]

School of Engineering, The University of Shiga Prefecture
[1]*Institute for Integrated Radiation and Nuclear Science, Kyoto University*

INTRODUCTION: To study the influences of ion irradiation induced damage on semiconductor surfaces at lower energies, we have prepared the plasma-exposed chips of the Si wafer as the samples. In the previous study using the oxygen plasma [1], we have observed almost no damages inside the sample surfaces. Because of the use of the oxygen, the Si surface was oxidized and the surface of the Si sample was covered with thin oxidized films. Therefore, the effect of the plasma treatment on Si substrate was not evaluated. In the present study, we have used the SF_6 gas to generate the plasma, and the effect of the damage induced during the etching of the Si surface was investigated by the S (line shape) parameter and the life-time measurement of the positron annihilation using the KUR slow positron beam system.

EXPERIMENTS: Chips of a Si (100) wafer with a size of about 18 mm × 18 mm were exposed to the RF (radio-frequency) plasma at a power of 5 W (#2, #3, #6, #7) or 40 W (#4, #5, #8, #9) with the oxygen gas pressure of 10 Pa (#2-#5) or 30 Pa (#6-#9) for 15 min. (#2,#4, #6, #8) or 30 min. (#3, #5, #7, #9). The sample of #1 was an untreated Si as a reference. For the measurement of the S parameters, slow positron beans at energies of 0 – 30 keV was used. Positron annihilation intensity at inter-lattice (I1) with bound electrons and inside damages (I2) with conduction electrons were obtained from the positron life-time spectra for each sample.

RESULTS: Fig. 1 shows the S parameters for the plasma treated, as well as untreated, Si wafer samples. In contrast to the oxygen plasma treated Si [1], S parameters at lower positron energies for plasma treated Si were increased, showing that the damages were induced to the surface region of the Si wafer during the plasma etching using the SF_6 gas. The S parameter of #2 (SF_6 gas pressure of 10 Pa) was larger than #6 (that of 30 Pa), which is because of the larger ion energies inside plasma for lower gas ambient in which the collision between ions (and/or radicals) are reduced in the lower density plasma.

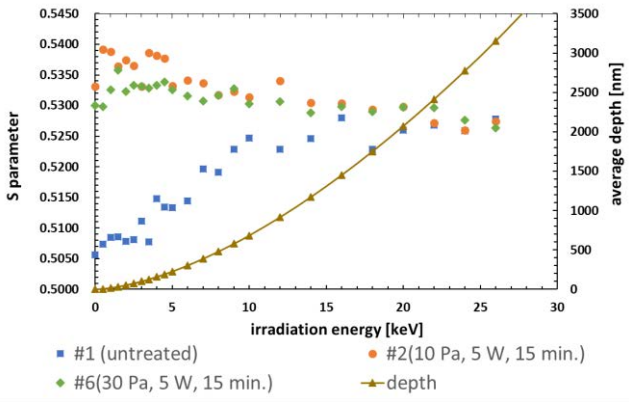

Fig. 1. S parameters for SF_6 plasma treated (#2, #6) and untreated (#1) Si wafer samples as a function of positron energy.

From the life-time measurement of the positron annihilation, the annihilation intensity of positrons at inter-lattice sites (I_1) and that at inside damages (I_2), such as vacancies and voids, can be obtained. The result is shown in Table 1. Although I_1 was far larger than I_2 for untreated Si (#1), as might be expected, the values of I_2 were increased to roughly about 6 - 7 times of that of I_1 after plasma treatment, indicating that the damages were surely induced by the plasma treatment used in the present study. For the sample #9, however, the value of I_2 was lower compared to other plasma-treated Si (#2 - #8). This might be because of the recovery of the induced damages due to the temperature-rise of the Si sample (*i.e.*, annealing effect) during the plasma treatment using the conditions of the plasma of higher RF power (40 W), higher SF_6 gas pressure (30 Pa), and longer process time (30 min.), used for #9.

Table 1. Annihilation intensities of positrons with electrons at inter-lattice (I_1) and inside damages (I_2).

sample	I_1 [%]	I_2 [%]
#1	93.27	6.728
#2	12.03	87.97
#3	14.64	85.36
#4	15.46	84.54
#5	11.94	88.06
#6	11.03	88.97
#7	12.89	87.11
#8	16.03	83.97
#9	19.82	80.18

CONCLUSION: After the SF_6-plasma treatment of Si wafer, damages of the etched surface was investigated using the method of the positron annihilations. It is found that both the value of the S parameter and the value of the annihilation intensity of positrons at inside damages were increased after the plasma treatment, indicating that damages, such as vacancies and voids, were induced inside the etched Si surfaces after the plasma treatment at conditions used in the present study.

REFERENCE:

[1] J. Yanagisawa, T. Furukawa, Q. Xu, A. Yabuuchi, K. Takamiya, and A. Kinomura, KURNS Progress Report 2020 (Kyoto University), CO4-6 (R2052).

CO4-12 Complex Structure of Ions Coordinated with Hydrophilic Polymer 22. Ionic Diffusion in Polymeric Structure Utilized by Polyiodide Ions. (3)

A. Kawaguchi and Y. Morimoto

KURNS

INTRODUCTION:

We have been investigating dynamical and interacted structures between iodine and polymers. Here, the term of "iodine" indicates not only simple I_2, but polyiodide ions (I_n^{m-}, *m, n*: integer, $n > 1$, "Poly-Iod" mentioned below) as charged molecules, which suggest concealed potential and diverse availability. [1,2]

While "Poly-Iods" are composed of iodine as unique element, their structure (atomic distance and charge distribution in one molecule) and coordination behavior between "Poly-Iods" can be widely modified corresponding to their environment. Occasionally, dipole or distributed positive charge (σ-hole) on "Poly-Iods" can be localized corresponding to their bonds with other atoms or ions. Or, though iodine is a member of halogen, mono-iodide ion, I^+, which does not belong to "Poly-Iods", can behave as single ion with positive charge. [3,4]

Such characteristic nature and ambiguity of iodine or "Poly-Iods" are also more emphasized in interaction with polymeric matrices or macromolecular environments. Experimental procedure for "iodine doping", which introduces "Poly-Iods" solved in solutions into the matrices advances through easy operation under normal pressure at room temperature. While various polymers (both natural and synthesized ones) can diffuse "Poly-Iods" into them and construct modified structure in which each matrix coordinates with "Poly-Iods", the structures as "iodine-doped" polymer often indicates paradoxical results as phenomena. For example, operation of "iodine doping" for polyamide-6 (PA6) introduces hardening and structuring as coordination of "Poly-Iods" with crystallite of PA6 or their re-orientation. On the other hand, simultaneously, operation also introduces softening or de-structuring as vanishing orientation or activation for ionic mobility. [5-7] Such paradoxical behaviors can be observed not only in PA6 matrix but also in other hydrophilic matrices such as poly vinyl-alcohol (PVA) or even in hydrophobic matrices. Furthermore, "Poly-Iods" even solved in aqueous solutions can interact with *hydrophobic* matrices. [8]

These paradoxical ambiguity indicated by "iodine-doping" process and following activity suggest that "Poly-Iods", which are surely charged molecules solved in aqueous solutions, may overcome division between hydrophilic and hydrophobic matrices restrictively.

DISCUSSION:

The most popular phenomenon as coordinated structure between "Poly-Iods" and polymer is "iodine-starch complex"; it is explained as coordination of starch as aqueously solved polymer with I_3^- or I_5^-.[9] On the other hand, existence of I_5^- or hydrophobic structure of helix chain of starch in the complex is not considered sufficiently. And, besides such aqueously solved polymer as host matrices, structure and functionality in matrices like as PA6 or PVA, which are hydrophilic and but unsolvable, should be complicated. Additionally, comprehensive explanation or theory have not be suggested yet.

Modestly saying, however, explanation should be offered beyond common dogma which may not be often considered strictly in chemistry. While chemical structure of monomer unit along polymer chain should be one of important information, it does not wholly dominate and explain characterization and functionality of polymeric system where hierarchic structures exist inevitably. There can be suggested "hydrophilicity or dipole in hydrophobic matrix" or "(localized) hydrophobicity in hydrophilic polymer".

In such microscopic environment presented for diffusion, simultaneous achievement for both coordination to fix ions with host matrices and dynamic transfer of substances through them can be suggested. It also means that "hydrophilicity vs. hydrophobicity of polymer" or "softening vs. hardening of result composite" should be discussed considering hierarchic structures in polymers.

Such ambiguous discussion which deviates from ordinary chemistry might be required for dynamics and structure in polymeric matrices. [to be continued]

ACKNOWLEDGMENTS: Some parts of these discussion are suggested by experimental results researched with Dr. Gotoh (Shinshu Univ.) and his staff and partially funded by NEDO.[2]

REFERENCES:

[1] patent. JPN-5444559 (2014).
[2] "Projects for Practical Use from Innovation" sponsored by NEDO (2007-2009).
[3] T.J. Marks & D.W. Kalina, "Extended Linear Chain Compounds" vol.1 ch.6., ed. J.S. Miller (Plenum Press, 1982).
[4] T. Clark, *et.al*., J Mol. Model, **13**, 291-296 (2007).
[5] A. Kawaguchi, Polymer, **35**, 3797-3798 (1994).
[6] KAWAGUCHI Akio, *et.al*., SPring-8 User Exp. Rep. **5** (2000A), 354-354 (2000).
[7] A. Kawaguchi, Sens. & Act. B, **73**, 174-178 (2001).
[8] A. Kawaguchi, Polym. Prep. Jpn., **62**,5116-5117 (2013).
[9] Rundle, R.E. and Baldwin, R.R., J. Am. Chem. Soc., **65**, 554-558 (1943).

CO4-13 Demagnetization Measurement of Permanent Magnet Materials Against Neutron Irradiation

Y. Fuwa[1], Y. Kuriyama[2], Y. Iwashita[2], K. Takamiya[2], and T. Takayanagi[1]

[1]*J-PARC Center, Japan Atomic Energy Agency*
[2]*Institute for Integrated Radiation and Nuclear Science, Kyoto University*

INTRODUCTION: In recent years, energy-saving has become one of the most critical issues for developments in particle accelerator research. The range of applications of permanent magnets in accelerators is expanding to reduce energy consumption. In addition to rare earth magnets with large remanent magnetization, the use of inexpensive ferrite magnets has been proposed [1,2].

One of the problems associated with applying permanent magnets in particle accelerators is demagnetization caused by radiation. Many research groups conducted experiments to evaluate the demagnetization for undulators in synchrotron radiation facilities [3], but the data has many discrepancies [4]. In addition, there is a lack of data on radiation demagnetization for ferrite magnets. Therefore, a more precise analysis of the radiation demagnetization is required for accelerators targeting higher beam intensities. Experiments have been carried out using the irradiation facilities of the KUR.

EXPERIMENTS: In this study, magnet samples were irradiated with up to 3 x 10^{19} n/cm^2 neutrons using a Pneumatic transport tube (Pn-2), a hydraulic transport tube (Hyd), and a long-term irradiation plug (LI). The rate of radiation-induced demagnetization was evaluated by comparing the remanent magnetization of samples before and after the irradiation. To measure the magnetization of the samples, we prepared a rotating stage for magnet samples and a Helmholtz-like pickup coil. By rotating the sample in the pickup coil, the voltage is induced in the coil. The measured amplitude of the induced voltage corresponds to the magnetization of the sample. This method made it possible to evaluate the amount of magnetization more precisely and in a shorter time than with a Hall probe [5,6].

RESULT AND DISCUSSION: Ferrite magnets (Y30H) and neodymium magnets (N35H, N40) were used as samples in this experiment. Fig. 1 shows the measured demagnetization rate as a function of irradiated neutron fluence [7]. For the ferrite magnets, 10% demagnetization was observed at a neutron fluence of 3 x 10^{19} n/cm^2. For neodymium magnets, it was confirmed that large demagnetization was observed up to an irradiation dose of 10 x 10^{16} n/cm^2. Comparing the results of N35N and N40, the magnitude of demagnetization differs by approximately a factor of two for the same amount of neutron irradiation. These results suggest that one of the reasons for the variation of data in previous studies may be that the samples with different compositions were treated the same. The temperature of the sample at the time of irradiation may also affect the degree of demagnetization. As a next plan, we plan to conduct experiments to systematically evaluate the effects of different material compositions and irradiation temperatures on demagnetization.

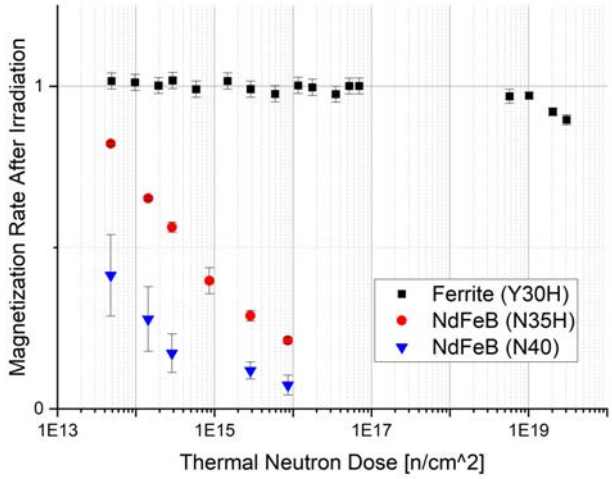

Fig. 1. Measured demagnetization rate for the samples of ferrite (Y30H), and neodymium magnets (N35H, N40).

REFERENCES:

[1] Y. Fuwa and Y. Iwashita, "Performance evaluation of a klystron beam focusing system with anisotropic ferrite magnet", Progress of Theoretical and Experimental Physics, 2017, 023G01.
[2] Y. Iwashita, M. Abe, T. Yako, Y. Fuwa and N. Terunuma, "Bipolar Correction Magnet With Permanent Magnets", IEEE Transaction on Applied Superconductivity, Vol. 30, No. 4, JUNE 2020, 4003703.
[3] [7] T. Bizen and H. Kitamuta, "Radiation-induced Demagnetization of Nd2Fe14B Magnets for Undulators" Journal of JSSRR, March 2004 Vol. 17 No. 2 pp. 53-58.
[4] X.-M. Maréchal, T. Bizen, Y. Asano, and H. Kitamura, "65 MeV Neutron Irradiation of Nd-Fe-B Permanent magnets", Proceedings of European Particle Accelerator Conference (EPAC) 2006, THPCH135, pp. 3116-3118 (2006).
[5] T. Yako, Y. Iwashita, M. Abe, T. Kurihara, M. Fukuda, M. Sato, T. Sugimura, Y. Fuwa, K. Takamiya, and Y. IInuma, "Measurement of Radiation Resistivity of Ferrite Permanent Magnets Irradiated by Neutrons", Proceedings of the 16th Annual Meeting of Particle Accelerator Society of Japan, 1003-1005 (2019).
[6] Y. Fuwa, Y. Kuriyama, and Y. Iwashita, "Magnetization Measurement Scheme for Radiation Demagnetization Evaluation of Permanent Magnets", Proceedings of the 18th Annual Meeting of Particle Accelerator Society of Japan, 58-60 (2021).
[7] Y. Fuwa, T. Takayanagi, Y. Kuriyama, Y. Iwashita, and K. Takamiya, "Radiation-Induced Demagnetization Measurement of Permanent Magnet Materials by Systematic Neutron Irradiation", 27th International Conference on Magnet Technology, TUE-P10-115-05 (2021).

CO4-14 Evaluation of Deuterated Macromolecular Crowder by Small Angle X-ray Scattering and Dynamic Light Scattering

Y. Nagata[1], M. Sugiyama[2], R. Inoue[2], N. Sato[2], and K. Morishima[2]

[1] *Institute for Chemical Reaction Design and Discovery, Hokkaido University*
[2]*Institute for Integrated Radiation and Nuclear Science, Kyoto University*

INTRODUCTION: A wide variety of biomolecules exist at high concentrations in the living cells and are thought to have a significant effect on the structure and dynamics of proteins. [1-3] Usually, measurement experiments on protein solutions are performed using dilute solutions (1 mg/mL or less). However, there is a large difference from the actual concentration (200 to 400 mg/mL) in the living cell. Therefore, it is quite important to reproduce the intracellular environment by adding various compounds (so-called crowders to reproduce the intracellular crowded system) at high concentrations to measure protein structure and dynamics under realistic conditions, and polymer crowders have been studied.

In this study, we focus on the preparation of polyethylene glycol (PEG) and deuterated PEG as macromolecular crowders to analyze their properties by small-angle X-ray scattering (SAXS) and dynamic light scattering (DLS) experiments.

EXPERIMENTS and RESULTS: Firstly, we have tried direct polymerization of 1,2-ethanediol in the presence of iodine according to the previous report. After the heating for 22 h at 190 °C, we obtained the corresponding oligomeric products (up to 5 mers) and could not obtained H-PEG (Scheme 1). [4]

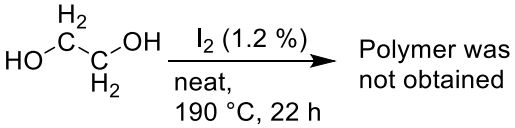

Scheme 1. Synthesis of a PEG from 1,2-ethanediol at 190 °C for 22 h.

We then tried a polymerization of ethylene sulfite in the presence of methyl trifluoromethanesulfonate according to a report (Scheme 2).[5]

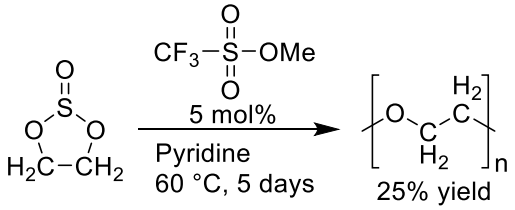

Scheme 2. Synthesis of PEG from ethylene sulfite at 60 °C for 5 days.

After 5 days at 60 °C, PEG was obtained at 25% yield. The number average molecular weight of the obtained PEG was estimated as 1140 (25.9 mers) based on the ^{1}H NMR analysis.

Subsequently, we tried to partially deuterated PEG, which is an important material for the contrast variation small-angle neutron scattering (SANS) measurements. 1,2-ethanediol and deuterated 1,2-ethanediol was converted to deuterated and non-deuterated 1,3,2-dioxathiolane 2-oxide, which were polymerized in the presence of methyl trifluoromethanesulfonate without purification (Scheme 3). We certainly obtained the partially deuterated PEG; however, the yield was insufficient (8.5%). Now we are optimizing the reaction conditions of this reaction to obtain partially deuterated PEGs with high yield to submit SAXS, DLS, and SANS experiments.

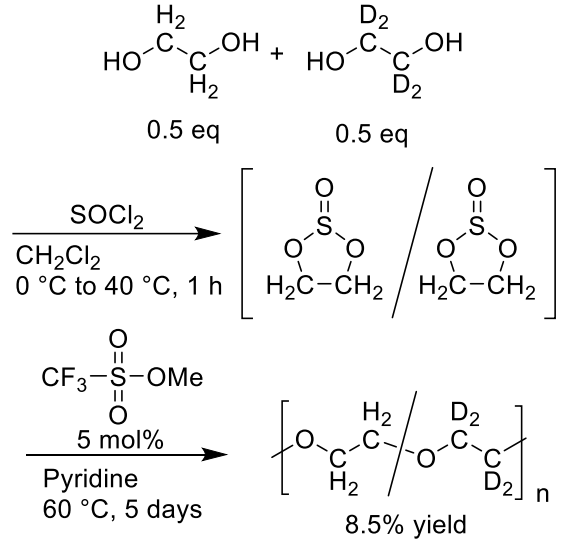

Scheme 3. Synthesis of a partially deuterated PEG from 1,3,2-dioxathiolane 2-oxide from 1,2-ethanediol and deuterated 1,2-ethanediol.

REFERENCES:

[1] Minton, A. P. Implications of macromolecular crowding for protein assembly. *Curr. Opin. Struct. Biol.* **2000**, *10*, 34-39.
[2] Ellis, R. J. Macromolecular crowding: an important but neglected aspect of the intracellular environment. *Curr. Opin. Struct. Biol.* **2001**, *11*, 114-119.
[3] Ellis, R. J. Macromolecular crowding: obvious but underappreciated. *Trends Biochem. Sci* **2001**, *26*, 597-604.
[4] Schnabel, R. Synthesis of Deuterated Polyethylene Glycols. *J. Label. Compd. Radiopharm.* **1992**, *31*, 91-94.
[5] Azuma, N.; Sanda, F.; Takata, T.; Endo, T. Effect of ring size on the cationic ring-opening polymerization of cyclic sulfites. *Macromol. Chem. Phys.* **1998**, *199*, 1785-1789.

CO4-15 TDPAC Measurement of ^{111}Cd(¬ ^{111}In) in Ultrafine Bubble Water

M. Tanigaki, D. Hayashi[1], Y. Ohkubo, A. Taniguchi, Y. Ueda[2], Y. Tokuda[3]

Institute for Integrated Radiation and Nuclear Science, Kyoto University
[1]Graduate School of Science, Kyoto University
[2]Research Institute for Sustainable Humanosphere, Kyoto University
[3]Depertment of Education, Shiga University

INTRODUCTION: Ultrafine bubbles, the gaseous cavities with diameters less than one micrometer, have recently attracted much attention because of their multifunctionalities [1]. While applications of ultrafine bubbles are extended in a wide variety of fields, fundamental studies on ultrafine bubbles themselves are not well extended because of their small size, smaller than the wavelength of radiant rays.

As we have previously shown in the internal pressure measurement of Xe-ultrafine bubbles [2], the perturbed angular correlation measurement is a useful technique for the study of the ultrafine bubble.

This time, the time differential perturbed angular correlation (TDPAC) of ^{111}Cd(¬ ^{111}In) in the aqueous solution with ultrafine bubbles is performed for the study of the interface of ultrafine bubbles, which should be one of the essential origins of its multifunctionality.

EXPERIMENTS: Typical four-counter TDPAC measurements were performed for the 171-245 keV cascade in ^{111}Cd(¬ ^{111}In) in aqueous solutions of pH = 2, 10, and 14 with/without Oxygen-ultrafine bubbles. The average diameter and the density of the ultrafine bubbles in each sample were 314 nm and 1.03 ×10^7/mL, respectively. ^{111}In was obtained from Nihon Medi-Physics as the aqueous solution of $^{111}InCl_3$ at the pH of approximately 2. This ^{111}In solution was added to each aqueous solution sample, followed by the pH adjustments by the appropriate addition of NaOH or HCl. For comparison, aqueous samples without ultrafine bubbles were also prepared in the same way. The angular correlation term $A_{22}G_{22}(t)$ is given by the following equation,

$$A_{22}G_{22}(\mathrm{t}) = \frac{2\left(N(180°,t)-N(90°,t)\right)}{N(180°,t)+2N(90°,t)},$$

where $N(90°, t)$ and $N(180°, t)$ are the counting numbers of the 171-245 keV γ-γ cascade at 90 and 180 degrees, respectively. Time-dependent term $G_{22}(t)$ for each sample was obtained by normalizing obtained $A_{22}G_{22}(t)$ by the asymmetry parameter of 171-245 keV cascade in ^{111}Cd, $A_{22} = -0.18$.

RESULTS: Demille reported a long relaxation time in the cases that either low (up to pH = 3.5) or high (between pH = 13 and 14) pH region, and an initial drop to a minimum at 15 to 20 ns and at later times a slow relaxation similar to that observed at extreme pH values in pH = 3.5~13. This pH dependence is understood as the quadrupole interaction in the symmetrical complexes $[In(H_2O)_6]^{3+}$ and $[In(OH)_6]^{3-}$ in extreme pH values, and the formation of less symmetrical complexes and tumbling aggregations at intermediate pH values [3].

Observed $G_{22}(t)$ in the present study well reproduced the results reported by Demille, and the initial drop at 15 to 20 ns in $G_{22}(t)$ at pH = 10 was more significant in Oxygen-ultrafine bubble water （Fig. 1). This difference may be caused by the interactions between the In complexes and the ultrafine bubbles. More studies, such as the detailed pH dependence, are underway.

The present work is supported by JSPS KAKENHI Grant Number 18K03948 and 21K03854.

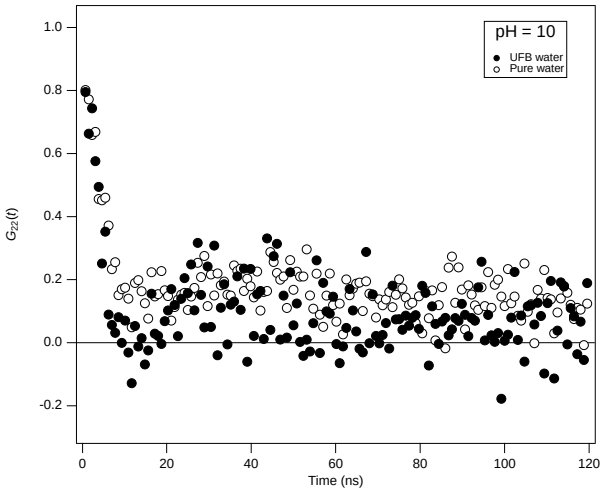

Fig. 1 TDPAC spectra of ^{111}Cd(¬ ^{111}In) in ultrafine bubble water and pure water at pH = 10.

REFERENCES:[1] E. G. Denis, The fine bubble breakthrough. https://www.iso.org/news/2014/05/Ref1844.html
[2] M. Tanigaki, T. Yamakura, Y. Ueda, A. Taniguchi, Y. Tokuda, and Y. Ohkubo, KURNS Progress Report 2018, p.31.
[3] G. R. Demille, D. L. Livesey, K. Mailer and S. P. Turner, Chemical Physics Letters, **44** (1976) 164‑168.

CO4-16 Tritium release behavior from neutron-irradiated FLiNaK mixed with Ti powder

K. Katayama, K. Kubo, T. Ichikawa, A. Ipponsugi, M. Oya, T. Takeishi[1], and Y. Iinuma[2]

Department of Advanced Energy Engineering Science, Kyushu University
[1]Faculty of Engineering, Kyushu University
[2]Institute for Integrated Radiation and Nuclear Science, Kyoto University

INTRODUCTION: In DT fusion reactors, understanding of tritium behavior is important from a viewpoint of safety. In the self-cooling liquid blanket concept tritium breeding material plays two important roles of tritium transport and heat transport. Tritium is produced in the breeding material by the nuclear reaction between neutrons and Li. Fluoride molten salts such as FLiNaBe and FLiBe are a promising liquid blanket material due to high stability at high temperatures, low reactivity with O_2 and H_2O, and low MHD pressure drop. Since fluoride molten salts have a low solubility for hydrogen isotopes, the produced tritium tends to release from the molten salt. This property means that tritium can be easily recovered from the molten salt but also a part of tritium is lost to the outside of cooling tubes by the permeation on the way to the tritium recovery system. For suppressing tritium loss by increasing effective solubility for tritium, the addition of Ti powder was proposed [1]. However, few studies on molten salt materials containing Ti powder have been performed. In order to control tritium safely and to design tritium recovery system, it is necessary to understand the fundamental behavior of tritium in the molten salt mixed with Ti powder. Since FLiNaBe and FLiBe contain highly toxic beryllium and is not easy to handle safety, FLiNaK is usually used as a simulated fluid. In this study, the solid state sample of FLiNaK mixed with Ti powder was irradiated by neutrons at Kyoto University Research Reactor, and tritium release behavior from the free surface of the molten salt by heating was observed in Kyushu University.

EXPERIMENTS: In the powders of LiF, NaF and KF were mixed in a Ni crucible under Ar atmosphere. The Ni crucible was put in the stainless-steel heating pot and repeatedly heated to 600 ℃ with Ar purging to remove impurity water vapor. The heating was repeated to homogenize the FLiNaK and the plateau region of temperature change was confirmed at at 454 ℃ which is melting point of FLiNaK. Ti powder was added to the part of FLiNaK with 2.5 wt% and it was heated with Ar purging. The prepared sample of FLiNaK was packed into quartz tubes in vacuum and it was installed into a polyethylene capsule. The thermal neutrons irradiation was performed by at pneumatic tube 2 (Pn-2) with the fluence of at Pneumatic Tube 2 (Pn-2) of the 1.7×10^{15} cm^{-2}.

Tritium release experiment was carried out in Kyushu University. The schematic illustration of experimental apparatus is shown in Fig.1 The irradiated sample was put in a Mo crucible and it was installed in the stainless-steel reaction tube. In order to melt the sample sufficiently, heating temperature was set to be to 600 ℃ or 700 ℃ with Ar purge. The chemical form of tritium released from the sample was expected to be TF and HT (T_2) and HTO (T_2O) and these were separately quantified. Details of the quantification method were described in Ref.2.

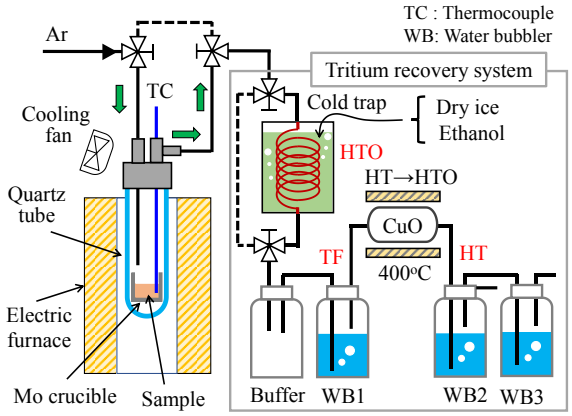

Fig.1 The schematic of experimental apparatus.

RESULTS: Fig.2 shows tritium desorption rate of HT and TF from neutron irradiated FLiNaK with 2.5 wt% Ti powder. It was found that most tritium was released as HT. A large difference was observed in the change of desorption rate between 600 ℃ and 700 ℃. It can be said that the lower the temperature, the higher the tritium absorption capacity of Ti, so that the amount of tritium transferred to Ti in FLiNaK increased and the release from the free interface was suppressed. Since tritium desorption from Ti is took place with decreasing tritium concentration in FLiNaK, the decreasing of the desorption rate was slow at 600 ℃. On the other hand, at 700 ℃, the amount of tritium absorbed in Ti is small, and the concentration of tritium in FLiNaK decreased rapidly, and the decreasing of the desorption rate was fast.

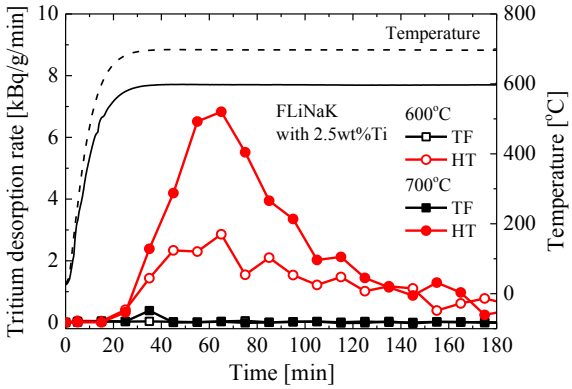

Fig.2 Tritium desorption rate at 600 ℃ and 700 ℃ from FLiNaK mixed with 2.5 wt% Ti.

REFERENCES:

[1] A. Sagara, *et al.*, Fusion Eng. Des. 89 (2014) 2114.
[2] K. Kubo, *et al.*, Fusion Eng. Des. 171 (2021) 112558.

CO4-17 Tritium recovery behavior for tritium breeder Li_4SiO_4 – Li_2TiO_3 biphasic material

Y. Oya[1], S. Hirata[2], Fei Sun[3], Yongjin Feng[4], Xiaoyu Wang[4], Hailiang Wang[5], M. Kobayashi[6], Y. Iinuma[7] and R. Okumura[7]

1 Faculty of Science, Shizuoka University
2 Graduate School of Integrated Science and Technology, Shizuoka University
3 School of Material Science and Engineering, Hefei University of Technology
4 Fusion Technology Research Division, Center for Fusion Science, Southwestern Institute of Physics
5 College of Physics, Sichuan University
6 National Institute for Fusion Science
7 Institute for Integrated Radiation and Nuclear Science, Kyoto University

INTRODUCTION: In the fusion blanket system, tritium (T) is produced by (n, α) reaction with lithium (Li). Li_2TiO_3 (LTO) and Li_4SiO_4 (LSO) are regarded as one of the promising solid breeder candidates. LTO has higher chemical stability, but the lithium density is not so high. On the contrary, LSO has higher Li density. Recently, LSO-LTO biphasic materials are proposed as advanced candidates to achieve high tritium breeder ratio (TBR) and quick T recovery at lower temperature by the combination of both LSO and LTO advantages. However, the T recovery performance was not well understood. In this study, LSO-LTO biphasic materials with various phase ratios were used and their tritium desorption behaviors after neutron irradiation was evaluated by T thermal desorption spectroscopy (T-TDS).

EXPERIMENTS: Three kinds of pebble samples with different phase rates, namely Li_4SiO_4-Li_2TiO_3 (LSO-LTO), $2Li_4SiO_4$-Li_2TiO_3 (2LSO-LTO) and Li_4SiO_4-$2Li_2TiO_3$ (LSO-2LTO) were fabricated at Southwestern Institute of Physics (SWIP) in China [1]. These samples were introduced in Kyoto University Research Reactor (KUR) to perform neutron irradiation. The thermal neutron flux was 5.50×10^{12} n cm^{-2} s^{-1} and the fluence was reached to be 7.96×10^{16} n cm^{-2}. After the neutron irradiation, T-TDS measurement was performed at Shizuoka University from R.T. to 1113 K with the heating rates of 5 - 30 K min^{-1}. After T-TDS, total T amount trapped by water bubbler was measured by a liquid scintillation counter.

RESULTS: Fig. 1 shows the T-TDS results. In this experiment, no HT was observed and almost all of T was released as HTO form. The major T desorption temperature was shifted toward lower temperature side as increasing the phase rate of LTO. For 2LSO-LTO sample, the T desorption was also observed at higher temperature side, but as increasing the phase ratio of LTO, these desorption peaks were disappeared. This is conceivable that the grain size is become smaller as increasing the content of LTO, which would affect the tritium desorption due to shorter diffusion distance. Table 1 summarizes the lithium density and the amount of desorbed T with chemical form of HTO and HT. It was clear that most of T was released as water form (HTO). The largest T retention was observed for 2LSO-LTO, and as the phase ratio of LTO increased, T retention was reduced, which was consistent with Li density in the samples. In addition, by increasing the phase ratio of LTO, T release temperature were shifted toward lower temperature side, indicating to the easy T recovery. Comparing of T-TDS spectra for biphasic LSO-LTO ceramic with monophase LSO or LTO, the shape of TDS spectra was close to that for LTO as increasing the phase rate of LTO. As the phase ratio of LSO was increased, T-TDS spectra was consistent with that for monophase LSO. [2,3] Therefore, it was concluded that LSO-LTO biphasic materials with the phase ratio of 1 : 1 has higher T recovery performance at lower temperature and good mechanical property.

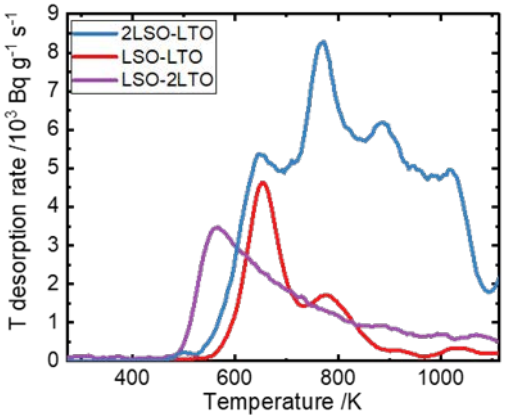

Fig. 1 T-TDS spectra of 2LSO-LTO, LSO-LTO and LSO-2LTO at 20 K min^{-1}.

Table 1 Li density and the amount of desorbed tritium.

Sample	Li density (g cm^{-3})	HTO (MBq g^{-1})	HT (MBq g^{-1})
2LSO-LTO	0.44	8.63	0.21
LSO-LTO	0.39	4.37	0.28
LSO-2LTO	0.35	3.27	0.12

REFERENCES:

[1] C. Dang *et al.*, J. Nucl. Mater. 500 (2018) 265-269.
[2] Qilai Zhou *et al.*, J. Nucl. Mater. 522 (2019) 286-293.
[3] Q. Qi *et al.*, J. Nucl. Mater. 539 (2020) 152330.

CO4-18 Vacancy migration energy in CrFeCoNi medium-entropy alloy

H. Araki, K. Sugita, M. Mizuno, A. Yabuuchi[1] and A. Kinomura[1]
Graduate School of Engineering, Osaka University
[1]*Institute for Integrated Radiation and Nuclear Science, Kyoto University*

INTRODUCTION: Tsai *et al*. [1] originally proposed the concept of sluggish diffusion, based on a positive correlation between the activation energies for atomic diffusion, which are normalized by the melting temperature, T_m , and the number of constituent elements in the CrMnFeCoNi high-entropy alloy(HEA) and its subsystems. However, the reason for the sluggishness of diffusion is not quite clear.

In the CrMnFeCoNi HEA and its subsystems at high temperatures, atomic diffusion is expected to proceed via a vacancy mechanism because they are substitutional solid solutions. Therefore, vacancy formation and migration energies in the CrMnFeCoNi HEA and its subsystems are important indexes for understanding the sluggish diffusion. In this work we have evaluated the vacancy migration energy in CrFeCoNi medium-entropy alloy by observing the vacancy migration and annihilation behavior during an annealing process after electron irradiation, with the use of the positron lifetime spectroscopy.

EXPERIMENTS: An arc-melted ingot of CrFeCoNi alloy was homogenized at 1373K for 24 h under argon atmosphere, and cut into 10 mm × 10 mm × 0.5 mm plates. The plates were polished and then sealed in silica tubes. Solution heat treatment was carried out for 1 h at 1373 K and the samples were quenched in water. Their X-ray diffraction analysis shows that all the samples are composed of single phase with a fcc structure. Then, the samples were irradiated in water with 8 MeV electrons at a fluence of approximately, 1×10^{22} e^{-} m^{-2} below 358 K using the electron linear accelerator at the Institute for Integrated Radiation and Nuclear Science, Kyoto University. The irradiated samples were isochronally annealed in a temperature range from 373 to 673 K. The temperature step during the isochronal annealing was 25 K and the duration of exposure to each temperature was 1 h.

The positron lifetime measurements were made at 297–299 K using a fast-fast timing coincidence system with a time resolution(FWHM) of 180–183 ps.

RESULTS: Before the electron irradiation the positron lifetime spectrum for the solution-treated alloys was represented by only one component of 108 ps, which is approximately equal to the values calculated for the defect-free constituent pure metals. This indicates that positrons annihilate in the bulk for the solution-treated alloy sample. After electron irradiation, the mean positron lifetime was increased to 133 ps. The analysis of positron lifetime spectra for the as-irradiated sample shows that many positrons are trapped and annihilate in the monovacancies introduced by electron irradiation, because the lifetime component, τ_2 , of trapped positrons was 180 ps, which is in agreement with the experimental values for monovacancies in the constituent pure metals. Assming that the specific trapping rate of monovacancies, μ_v , is 10^{15} s^{-1}, the vacancy concentration in the as-irradiated sample is of the order of a few atomic parts per million.

Fig.1 shows the change in the vacancy concentration during the isochronal annealing of the irradiated sample, which was evaluated on the basis of the two- or three-component analyses for the positron lifetime spectra. In the temperature range where dislocations and monovacancies are expected to coexist, the positron lifetime spectra were analyzed on the assumption that the positron lifetime component of dislocation is 150 ps. As shown in Fig.1, the vacancy concentration decreases with annealing temperature, because the vacancies introduced by electron irradiation gradually disappear as the vacancies become mobile during the isochronal annealing. The decrease in the vacancy concentration was theoretically analyzed on the basis of Dryzek *et al*.'s model for isothermal annealing [2] .

Assuming that the vacancy migration energy is constant over the whole temperature range, there remains a few discrepancies between the theoretical fitting model and the experimental data, as shown in Fig.1. The positron lifetime measurements indicate that dislocation loop components are detected in addition to vacancies at high temperatures, suggesting that the vacancy migration process is easily influenced by the presence of dislocations. Therefore, we assumed two-component vacancy migration energies (H_m^L , H_m^H) and optimized their values to fit the experimental data. The value of H_m^L obtained in the low temperature range is 0.92 eV, which is nearly equal to 0.93 eV of vacancy migration energy in CrMnFeCoNi [3].

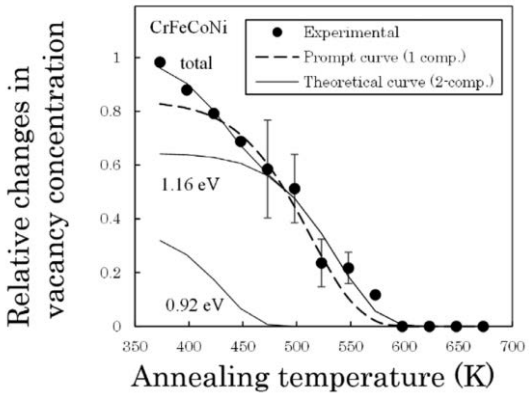

Fig. 1 The relative changes in vacancy concentration obtained from experiments and theoretical calculations.

REFERENCES:

[1] K. Y. Tsai, M. H. Tsai and J. W. Yeh, Acta Mater., **61** (2013) 4887.
[2] J. Dryzek, C. Wesseling, E. Dryzek and B. Cleff, Mater. Lett., **21** (1994) 209.
[3] K. Sugita, R. Ogawa, M. Mizuno, H. Araki and A. Yabuuchi, Scripta Materialia, **208** (2022) 114339.

CO4-19 A study on destruction of cesium aluminosilicate compounds by gamma irradiation (3)

H. Ohashi, R. Tawatari, T. Saito[1]

Faculty of Symbiotic Systems Science, Fukushima University
[1]KURNS

INTRODUCTION: Pollucite which is one of cesium aluminosilicate compounds have attracted attention as a final storage material of ^{134}Cs and ^{137}Cs. Pollucite is able to synthesized by hydrothermal method in low temperature below 300°C [1]. Pollucite has various properties that favor the immobilization of Cs ions.

However, the damage to the aluminosilicate framework by radiation decay is concerned because it contains ^{134}Cs and ^{137}Cs. It has been reported that the effect of β-ray emission and nuclide conversion by β-decay of ^{137}Cs on aluminosilicate framework is minor [2, 3]. On the other hand, there are few reports of effects by gamma rays on pollucite framework. Therefore, we examined the effect of gamma radiation on the aluminosilicate framework of Pollucite.

EXPERIMENTS: Potassium aluminate, potassium metasilicate and cesium chloride were dissolved in potassium hydroxide solution. The solution was placed in a Teflon inner cylinder pressure container. Pollucite was synthesized by hydrothermal method, holding the container at 180°C for 48 hours. The resulting precipitate was washed by distilled water. Thereafter, each solid was collected by filtration and dried at 110 °C for 12 hours or more. After that, each dried solid was stirred and washed using 0.1 mol dm^{-3} HCl and NH_4Cl for a day, respectively.

The powder samples were characterized by XRD, and gamma-irradiated at 0 and 100 kGy by ^{60}Co source. The leaching test by PCT-A method [4] was carried out to evaluate the change of Cs retention performance by framework damage. Concentration of cesium in solution leached was estimated by Ge Semiconductor Detector and atomic absorption spectrophotometry

RESULTS: All the XRD patterns of powders prepared were demonstrated that they were pollucite, and all the patterns showed that they contained only single-phase pollucite. The leaktests have been studied and we estimated that amount of leached cesium from samples with and without ^{60}Co-irradiation were over 10 ppm Cs. It was quite higher than those measured by other researchers[5]. Then, each dried solid was washed using 0.1 mol dm^{-3} HCl and NH_4Cl. The results for leaktests were shown in Table 1. The concentration of cesium ions leaked from pollucite was 10-15 ppm Cs. It was comparable with that at last year. The reason why the cesium ion concentration decreased by washing was due to the excessive adsorption of cesium ions on the sample surface. The washing process has proved to be very im-portant in preparing the final disposal material.

In our previous study, the irradiated pollucite sample showed little difference from the non-irradiated one in the amount of leached cesium. There were no effects of γ-ray on the aluminosilicate framework of pollucite in these experiments.

Table 1 Results for PCT-A-like leaktest.

sample	T (°C)	t / hr	Leakage rate	Method
Fukushima polluted soil	**90**	**40**	**0.126%**	**Ge Semiconductor Detector**
Pollucite	**90**	**40**	**0.034%**	**AAS**

REFERENCES:

[1] Y. Yokomori *et al.*, *Sci. Rep.*, **4** (2014), 4195
[2] J. Fortner *et al*., Argonne National Laboratory, Argonne, Illinois 60439 (2001).
[3] N. J. Hess *et al.*, *J. Nucl. Mater.*, **281** (2000), 22-33.
[4] ASTM C 1285-02 (2008).
[5] Z. Jing *et al.*, *J. Hazard. Mater.*, **306** (2016), 220–229.

CO4-20 Study on HPLC Elution Behavior of Heavy Lanthanide Metalloufullerenes

K. Akiyama[1], S. Nishimura[1], T. Kuroda[1], K. Takamiya[2], and S. Kubuki[1]

[1]*Department of Chemistry, Tokyo Metropolitan University*
[2]*Institute for Integrated Radiation and Nuclear Science, Kyoto University*

INTRODUCTION: Metallofullerene (EMF) is a clathrate compound encapsulating metal atom in fullerene molecule. Lanthanide (Ln) EMFs: $Ln@C_{82}$ have two or three charge transferred electrons on the C_{82} cage from the encapsulated Ln atom, and their electronic states reflecting the number of charge transfer electrons [1]. From the view point of inorgnic chemistry, It is interesing to know that the effect of the electronic state for a series of the encapsulated 10 lanthanide elements (La, Ce, Pr, Nd, Gd, Tb, Dy, Ho, Er, Lu) with the electronic states of $(Ln^{3+})@(C_{82}^{3-})$ on the electronic state of the $Ln@C_{82}$ molecule from the difference in interaction with pylenyl stationary phase. So far, we have made clear the retention time in the pyrenyl stationary phase for five types of $Ln@C_{82}$ from La to Gd by the thermal neutron activation method. On the other hand, the HPLC retention time of $Ln@C_{82}$ with heavy lanthanide elements have not been obtained because the half-life of the radio nuclide produced by thermal neutron irradiation such as Dy and Er is very short, and the interference by the production of $Ln_2@C_{82}$ and $Ln_2C_2@C_{80}$, whose production rate increase competitively with $Ln@C_{82}$ as the increase of the atomic number of Ln. In this study, we used already purified $Ln@C_{82}$ of heavy lanthanide by HPLC column of a 5PBB for the neutron activation and developed at three different temperature using newly developed column cooler to obtained detailed HPLC retention time of these $Ln@C_{82}$s.

EXPERIMENTS: The $Ln@C_{82}$ (Ln = La, Pr, Dy, Ho, Er) studied in this work was produced by the arc discharge method (DC 60 A) at 50 kPa under He atmosphere. The MF component was extracted from the crude fullerene extract obtained by arc discharged soot by an oxidation method using $TiCl_4$ [2]. After that, the extracts were injected into a HPLC column of 5PBB (eluent: toluene, flow rate: 6.0 ml/min) for the isolation of $Ln@C_{82}$s. These isolated $Ln@C_{82}$ were separately sealed into polyethylene vial and activated by a thermal neutron in the KUR of the Institute for Integrated Radiation and Nuclear Science, Kyoto university. After the irradiation, these samples were mixed and developed into a Buckyprep column (eluent: toluene) with a flow rate of 3.2 mL/min at 20 ºC (room temperature), 0 ºC, and -10 ºC to obtain the radiochromatogram.

RESULTS: Figure 1 shows the radiochromatogram of $Ln@C_{82}$ obtained at 20 ºC, 0 ºC, and -10 ºC together with HPLC chromatogram monitored by UV absorption. For each temperature, elution peak of $Ln@C_{82}$ was observed around 60 min., 75 min., and 85 min., respectively. Some data, such as Pr, were found to be not enough statistics. However, we have succeeded to obtain relatively good chromatogram for some of the targeted heavy lanthanide metallofullerenes. In the near future, improvements such as increasing the sample weight will be attempted to acquire data in addition to heavy lanthanoids, such as Ce, Nd, Tb, and Lu, for which data has not been acquired in this time.

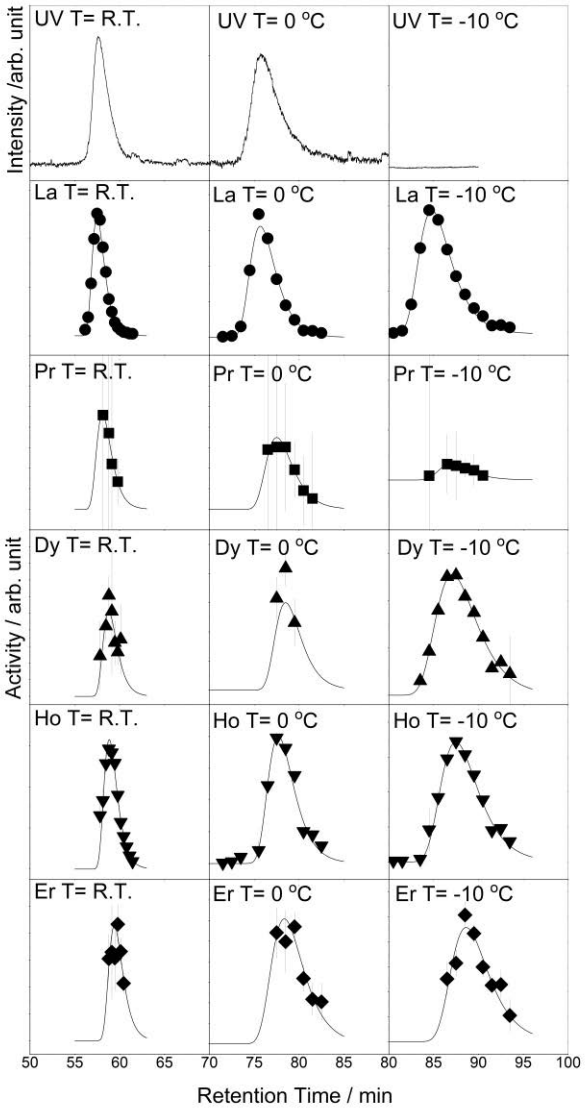

Fig. 1. Radiochromatogram of studied $Ln@C_{82}$ obtained at 20 ºC, 0 ºC, and -10 ºC, respectively. Solid lines of radiochromatogram in this figure indicates the result of least square fit of the data.

REFERENCES:

[1] H. Shinohara, Rep. Prog. Phys. **63** (2000) 843-892.
[2] K. Akiyama *et al.*, J. Am. Chem. Soc., 134 (2012) 9762-9767.

CO4-21 Glass compositional dependence of radiophotoluminescence in Cu-doped aluminoborosilicate glass

Y. Nishi, A. Kinomura[1], T. Saito[1], A. Okada[2], T. Wakasugi[2], K. Kadono[2]

Graduate School of Science and Technology, Kyoto Institute of Technology
[1]Institute for Integrated Radiation and Nuclear Science, Kyoto University
[2]Faculty of Materials Science and Engineering, Kyoto Institute of Technology.

INTRODUCTION: Radiophotoluminescence (RPL) is an emission from luminescent centers that are generated in materials by exposure to ionizing radiation. Recently, we have reported that Cu-doped aluminoborosilicate and silica glasses exhibit prominent RPL [1, 2]. The RPL mechanism of these glasses are explained as follows. First, ionizing radiation generates electron-hole pairs in the Cu-doped glasses,

$$\text{Glass} \rightarrow h^+ + e^-. \quad (1)$$

Then, the electrons are trapped at Cu^{2+} ions, and the Cu^{2+} ions are converted to Cu^+ ions, which emit bright luminescence in the visible region by UV excitation,

$$Cu^{2+} + e^- \rightarrow Cu^+. \quad (2)$$

The reverse reaction, in which Cu^+ ions trap holes and are converted to Cu^{2+} ions, may also occur,

$$Cu^+ + h^+ \rightarrow Cu^{2+}. \quad (3)$$

This reaction (3) reduces the RPL centers. Therefore, in the Cu-doped glasses, the RPL is induced by the progress of reaction (2). In this RPL mechanism, the concentration ratio of Cu^+ and Cu^{2+} ions, and the concentration of Cu^+ ions in glasses are important to observe remarkable RPL. The amount of Cu^+ ions should be less than that of Cu^{2+} ions, and it is better that the concentration of Cu^+ ions is as low as possible. It is well known that the concentration ratio of Cu^+ and Cu^{2+} ions are strongly dependent on the components and compositions, and the preparation conditions of glasses. Thus, we have investigated the relationship between the RPL behaviors, and the glass systems and compositions. Here, we present a new composition of the aluminoborosilicate glass which exhibits more prominent RPL than the previously reported one [1].

EXPERIMENTS: The compositions of the prepared glasses are $25Na_2O \cdot 25Al_2O_3 \cdot 10B_2O_3 \cdot 40SiO_2$ (mol%) (ABS25) and $30Na_2O \cdot 20Al_2O_3 \cdot 10B_2O_3 \cdot 40SiO_2$ (ABS30); the former is the composition previously reported [1] and the latter is a new composition. The concentration of copper incorporated into these glasses was 5 mmol% of Cu to 100 mol% of the host glasses. Obtained glasses were cut to 1.0 mm in thickness and both sides were optically polished.

X-ray and γ-ray irradiations of the glasses were performed using an X-ray fluorescence spectrometer equipped with an X-ray source with a Rh target, and the ^{60}Co gamma-ray irradiation facility in the Institute for Integrated Radiation and Nuclear Science, Kyoto University, respectively. Both irradiations were performed at room temperature.

RESULTS: Figure 1 shows the emission spectra of the Cu-doped glasses before and after the X-ray irradiation. Before the irradiation, a weak emission assigned to the transition from $3d^9\ 4s^1$ to $3d^{10}$ of Cu^+ is observed for the ABS25 glass whereas the emission is hardly detected for the ABS30 glass. This means that the ABS30 glass contains almost no Cu^+ ions whereas some amount of copper ions in the ABS25 glass present as Cu^+ ions [1]. This is due to the difference in the basicity of glass; in the glasses of higher basicity, the redox equilibrium between Cu^{2+} and Cu^+ ions shifts to the oxidation side, i.e., the side of Cu^{2+}. After the irradiation, the intensity of the emission remarkably increased. The emission intensity of the ABS30 glass after the irradiation is almost the same as that of the ABS25 glass. Therefore, the ABS30 glass is a material that exhibits a more prominent RPL behavior.

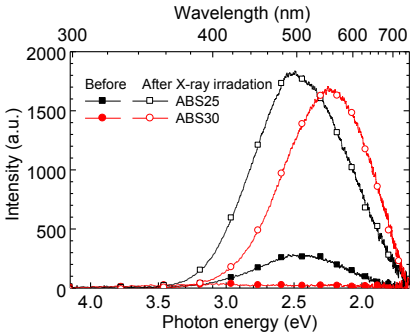

Figure 1 Luminescence spectra of Cu-doped aluminoborosilicate glasses before and after X-ray irradiation.

In order to investigate the relationship between the luminescence intensity and the irradiation dose, the Cu-doped ABS30 were exposed to various doses of γ rays. Figure 2 shows the dependence of RPL intensity on the γ-ray irradiation dose. The RPL intensity increased even at 10 Gy or less. The inset show that the RPL intensity proportionally increased with the γ-ray dose until about 300 Gy and then tended to be deviated from the proportionality. This value is much higher than that reported for the Ag-activated aluminophosphate glasses used for personal dosimeters.

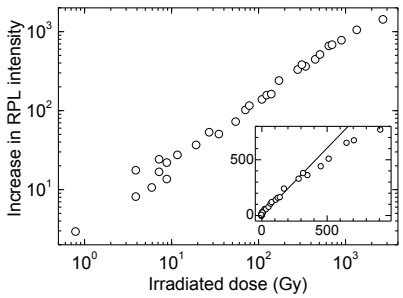

Figure 2 Dependence of RPL intensity of Cu-doped ABS30 glass on irradiation dose after exposure to ^{60}Co γ-rays. Irradiation dose is represented as absorption dose for water.

In conclusion, the Cu-doped aluminoborosilicate glass is promising for dosimeters used in environments under the relatively high irradiation doses.

REFERENCE:

[1] H. Hashikawa, *et al.*, *J. Am. Cer. Soc.*, **102**(4), 1642-1651 (2019).
[2] Y. Takada, *et al.*, *AIP Adv.*, **11**(3), 035208 (2021).

CO4-22 Formation of radiation defects on tungsten and their influence on effect of hydrogen isotope retention

K. Tokunaga, M. Matsuyama[1], M. Hasegawa,
K. Nakamura and Q. Xu[2]

Research Institute for Applied Mechanics, Kyushu University
[1]Hydrogen Isotope Research Center, University of Toyama
[2]Institute for Integrated Radiation and Nuclear Science, Kyoto University

INTRODUCTION: It is of a great importance to clarify phenomena of implantation, retention, diffusion and permeation of tritium (T) on surface of the armor materials of the first wall/blanket and the divertor on fusion device from a viewpoint of precise control of fuel particles, reduction of tritium inventory and safe waste management of materials contaminated with tritium. Refractory metals such as tungsten (W) is potential candidate for the armor of the first wall and the divertor plate of the fusion reactor because of its low erosion yield and good thermal properties. The armor material will be subjected to heavy thermal loads in the steady state or transient mode combined with high energy neutron irradiation that will cause serious material degradation. In addition, high energy runaway electrons would bombard the armor materials along the equatorial plane in fusion device. It is considered that these cause radiation damage and enhance tritium retention. In the present works, T exposure experiments have been carried out on W samples which were irradiated by high energy electrons to investigate effects of high energy electrons irradiation on microstructure and tritium retention of W. In this fiscal year, pure W and recrystallized W were irradiated by high energy electron beam. Before and after that, positron annihilation experiment was carried out to identify the radiation defect. In addition, EBSD（Electron Back Scatter Diffraction Patterns）analyses has been carried out on the specimens before and after the electrons irradiation. Tritium exposure experiments have been carried out using a tritium (T) exposure device.

EXPERIMENTS: W samples used were ITER specification W (ALMT-grade) (SR-W) and its recrystallized W (RC-W). The SR-W was fabricated via a powder metallurgical route including cold isostatic pressing, sintering, hot rolling, and heat treating to relieve the residual stresses. Some of the machined SR specimens were subjected to a full recrystallization treatment at 2000 ºC for 1 hr in vacuum. Sizes of the specimens were 10 mm x 10 mm x 1mm (10 mm x 10 mm : ND-TD). The surface of the both samples were polished to be mirrored. High energy electrons irradiation has been carried out using LINAC in Institute for Integrated Radiation and Nuclear Science, Kyoto University. An peak energy of electron irradiated was 8 MeV and DPA was 5.8 x 10^{-3}. Temperature during the irradiation was measured by thermocouples which was contacted with a backside of the W samples. Before and after that, positron annihilation experiment was carried out to identify the radiation defect. In addition, a high energy ion irradiation experiment has stared to carry out. The sample surface was irradiated by 2.5 MeV Fe ions with a flence of 5 x 10^{18} ions/m^2 at RT. T exposure experiments have been carried out using a T exposure device in University of Toyama. Pressure of the T gas was 1.3 kPa and T exposure was kept for 4 h at 100 ºC. T concentration in the gas was about 5 %. After the exposure to T gas, T amount retained in surface layers of the sample was evaluated by imaging plate (IP) measurements and β-ray-induced X-ray spectrometry (BIXS).

RESULTS: In the condition of 8 MeV electrons irradiation, the electron beams go through in 1 mm thickness W sample. On the other hands, damage by the Fe ion beam irradiation is very thin surface layer (a few μm). However, DPA of the damage area of the Fe ions irradiation is larger than that of the electron irradiation. Figure 1 shows the result of the IP measurement. The amount of T of the specimen surfaces evaluated by comparison with the standard samples is shown as Figure 2. These results indicate that the amount of T of the specimens irradiated by the electron and the Fe ion beams increases comparing with un-irradiated specimens. Quantitative evaluation is currently underway.

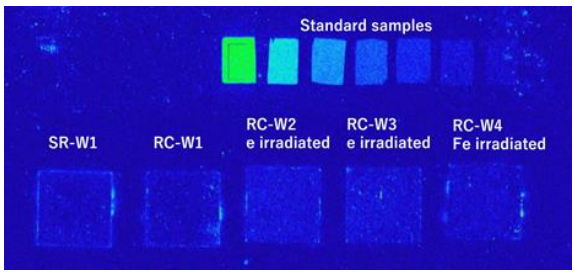

Figure 1 Result of IP measurement.

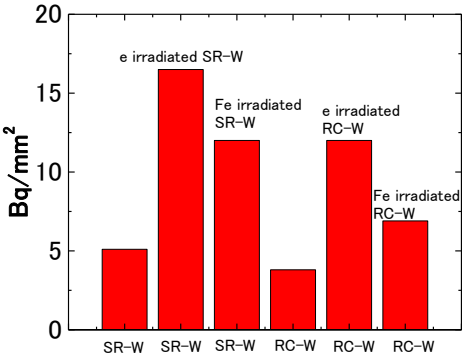

Figure 2 Amount of tritium on before and after electron and Fe ion irradiation measured by IP measurement. SR-W and RC-W are stress relief and recrystallized state, respectively.

CO4-23 Neutron irradiation tests for ITER plasma diagnostics

M. Ishikawa, T. Ushiki, E. Yatsuka, T. Yokozuka, H. Murakami, T, Kikuchi, K. Nojiri and T. Hatae

National Institutes for Quantum Science and Technology

INTRODUCTION: ITER [1] is being built in France by international cooperation. This study focuses on neutron irradiation effects on optical elements used in Dignostics for ITER. Expected 1 MeV Silicon equivalent fluence is 10^{12}-10^{15} n/c m^2 depending on locations of components. In order to investigate the effect of such high fluence on the actual components in a short time, neutron irradiation was performed using the slant exposure tube and the pneumatic tubes of the KUR. This report mainly presents, (1) effect of neutron irradiation of Silicon (Si) which is candidate material for optical lens of Infrared Thermography (IRTh) system and (2) briefly summarize the test results for the Edge Thomson Scattering system (ETS).

(1) Irradiation Tests of Si for Optical Lens of IRTh

IRTh will use Si lens in the ITER environment. Recent gamma-ray irradiation tests conducted by the authors show that the transmittance of Si is not significantly degraded by gamma-ray irradiation. However, some studies suggest that strong neutron irradiation induce several absorption bands in the wavelength range of IRTh (1.5 μm-4.5 μm) [2]. This study investigated threshold value of the total neutron dose for keeping transmittance of Si.

EXPERIMENTS: The slant exposure tube and pneumatic transportation facility was used for irradiation test of Si samples. In this test, several Si samples were irradiated in several neutron fluence up to 1.0 x 10^{17} (n/cm^2).

RESULTS: Figure 1 shows the irradiation test result of Si samples. As shown in Figure 1, the two fatal absorption bands (near-edge (less than 1.2 μm) and 1.78 μm) were induced by neutron irradiation. Figure 2 shows dependence of transmittance degradation of Si on neutron fluence. Absorption of near-edge (1.2 μm) and 1.78 μm exponentially increased from neutron fluence of 5.0 x10^{15} (n/cm^2). Judging by these results, the author concluded that Si lens unit can survive in ITER environment if neutron fluence at the location of lens unit can be decreased to about 2.5 x 10^{15} (n/cm^2) by shielding design. This value can be easily achieved by shielding of 20 cm-thick Boron carbide.

(2) Irradiation Tests of Optical Fibers of ETS

EXPERIMENTS: An optical fiber (hydrogen loaded fiber) that transmits the signal light of ETS was irradiated up to 9x10^{14} cm^{-2} for fast neutron and 8x10^{15} cm^{-2} for thermal neutron, which is equivalent to the 20-year cumulative fluence of the most severely irradiated areas of fibers of ETS in ITER. The performance deterioration due to neutron irradiation was investigated by comparing the wavelength dependence of transmitted signal before and after irradiation.

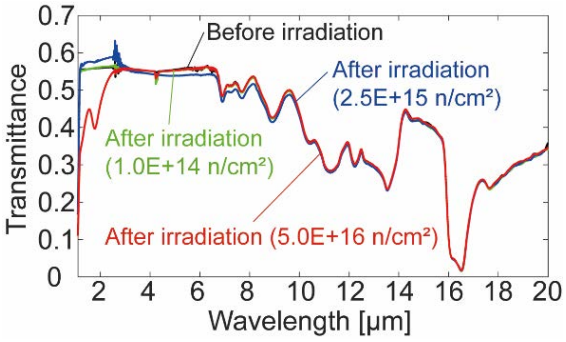

Fig. 1: Irradiation test result of Si samples.

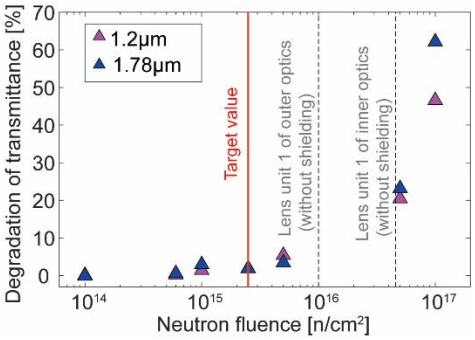

Fig. 2: Dependence of transmittance degradation of Si on neutron fluence.

RESULTS: Wavelength dependences of the signal before and after irradiation were compared. When normalized by the signal intensity of 743 nm, which was the peak value, the wavelength dependence of the signal was almost unchanged before and after neutron irradiation. It is unlikely that the transmittance was uniformly deteriorated in a wide wavelength range. This result indicates that it is highly possible that the spectral transmittance is not deteriorated by neutron irradiation in ITER.

ON GOING INVESTIGATIONS AND PROSPECTS:

The neutron irradiation test of grass materials (KU-1, KUVI) which will be used as vacuum window of Divertor Impurity Monitor was performed and the effect of the neutron irradiation on spectral transmittance is being investigated.

The preamplifier of Microfission Chamber (MFC) amplifies and converts the weak signal from the MFC detector into a nose tolerant strong output. The preamplifier will be installed in the port cell area and maximum neutron flux at the installation position of the preamplifier could become about 2.0 x 10^6 n/cm^2s. However, the effects on neutrons have not been evaluated yet. Therefore, in order to evaluate how much neutron shielding is needed neutron irradiation tests on the preamplifiers will be conducted in 2022

REFERENCES:

[1] B. Bigot, Fusion Eng. Des., **146**, 124 (2019).

[2] L. J. Cheng and J. C. Corelli, Phys. Rev. 152, No.2, 761-774 (1966).

CO4-24 Vacancy Formation by Al Doping in β-$FeSi_2$ Studied by a Reactor-Based Slow Positron Beam

A. Yabuuchi

Institute for Integrated Radiation and Nuclear Science, Kyoto University

INTRODUCTION: β-$FeSi_2$ is expected as an environmentally friendly infrared luminescent material. However, further enhancement of luminescence intensity is desired for practical use. Doping of β-FeSi2 with Al atoms which substitute Si sites has been reported to enhance the luminescence intensity [1]. The enhancement of luminescence intensity was considered to result from the filling of Si vacancies with Al atoms. In this study, defects in β-FeSi2 thin films doped with Al atoms occupying Si sites and Mn atoms occupying Fe sites were investigated with a slow positron beam.

EXPERIMENTS: Undoped, Al-doped, and Mn-doped β-$FeSi_2$ films were prepared by the ion-beam synthesis method [1]. Each sample is expected to have a β-FeSi2 layer with a thickness of around 60 nm on the surface of the Si substrate. These samples were probed by a slow positron beam at the Kyoto University Research Reactor [2]. The Doppler broadening of annihilation radiation (DBAR) spectra were acquired. All samples were treated with dilute hydrofluoric acid to remove oxide films before measurement. The shape of the obtained DBAR spectra was characterized in terms of the *S*-parameter [3], which depends on the fraction of positron annihilation with low momentum electrons.

RESULTS: Figure 1 shows *S*-parameters as a function of incident positron energy for each sample. The Al-doped sample shows an increase in *S*-parameters. This indicates that Al doping leads to the formation of vacancies. Figure 2 shows the positron implantation profile when positrons are implanted into β-$FeSi_2$ with an energy of 3 keV. The incident positron energy was fixed at 3 keV to probe the β-$FeSi_2$ layer formed on the Si substrate surface of each sample, and the coincidence DBAR spectra were acquired. Figure 3 shows the coincidence DBAR spectra of each sample normalized by that of the reference sample (Si), called the ratio curves. The peak around $11\times10^{-3}m_0c$ is reduced in the Al-doped sample, indicating that the spectral shape is closer to that of Si. This means that the vacancies contained in the Al-doped sample are Fe vacancies. Contrary to the previously considered hypothesis, Al-doping was found to result in the formation of Fe vacancies.

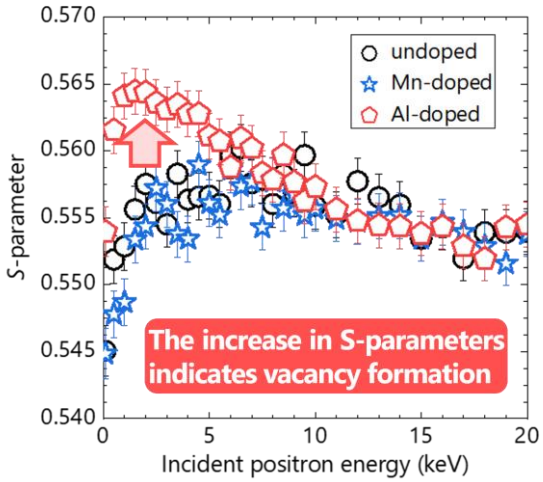

Fig. 1. *S*-parameters as a function of incident positron energy for each sample.

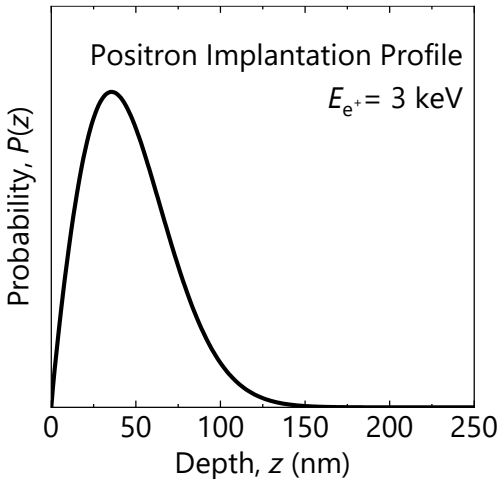

Fig. 2. Implantation profile of positrons implanted into β-$FeSi_2$ with an energy of 3 keV.

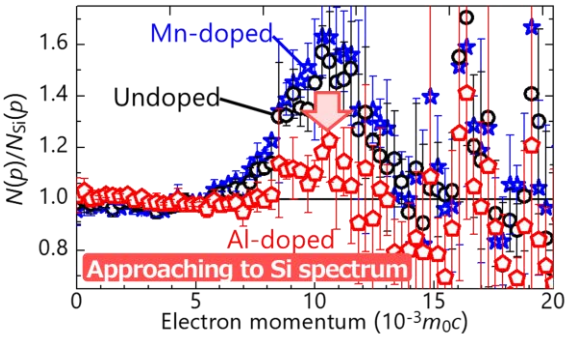

Fig. 3. Coincidence DBAR spectra obtained for each sample at incident positron energy of 3 keV. Each spectrum is normalized by that of Si.

REFERENCES:

[1] Y. Terai and Y. Maeda, Appl. Phys. Lett., **84** (2004) 903.

[2] A. Yabuuchi, Nucl. Instrum. Method Phys. Res., Sect. B **513** (2022) 44.

[3] F. Tuomisto and I. Makkonen, Rev. Mod. Phys. **85** (2013) 1583.

CO4-25 Change in Fe valence state of Fe and Ni substituted Li_2MnO_3 positive electrode material during different charge and discharge depths by ^{57}Fe Mössbauer spectroscopy

M. Tabuchi and Y. Kobayashi[1]
National Institute of Advanced Industrial Science and Technology (AIST)
[1]Kyoto University Institute for Integrated Radiation and Nuclear Science

INTRODUCTION: The Fe and Ni substituted Li_2MnO_3 (present composition: $Li_{1+x}(Fe_yNi_{0.3-y}Mn_{0.7})_{1-x}O_2$, $0<x<1/3$) is an attractive positive electrode material for next-generation and large-scale lithium-ion battery (LIB) [1]. To use it for LIB to the electric vehicle (EV), minimizing Ni content and utilizing Fe as redox center are necessary to avoid the risk of depletion for Ni source.

To accomplish above subject, understanding Fe valence change during different charge and discharge depths is needed by ^{57}Fe Mössbauer spectroscopy.

EXPERIMENTS: The sample was prepared by co-precipitation-calcination method. Water-soluble Fe, Ni and Mn salts dissolved in distilled water and dripped into NaOH solution at +20°C for 2-3 h. The coprecipitate was aged and oxidized by bubbling with O_2 flow for 2 days. The product was washed with distilled water and then was filtered. It mixed with Li_2CO_3 (Li/(Fe+Ni+Mn)=2) into distilled water to make homogeneous slurry. The dried slurry was used as a precursor. The precursor was powdered using vibration mill and then was calcined at 650 °C for 5h in air. The product was milled again and calcined at 850 (y=0.15 and 0.20) or 900 °C (y=0.10) for 5h in air or N_2 flow. After each calcination, the product was washed with distilled water and then continue to the filtration and drying processes.

The samples were characterized by X-ray diffraction (XRD), chemical analysis and half-cell tests. The lithium metal and 1.5 M $LiPF_6$ EC-DMC (3:7) used as anode and electrolyte, respectively. The velocity axis of ^{57}Fe Mössbauer spectra was calibrated by α-Fe.

RESULTS: The XRD patterns for all samples can be indexed by monoclinic Li_2MnO_3-type structure (*C*2/*m*). The crystallographic parameters depend on calcination atmospheres even at same transition metal (TM) ratio; the lattice parameters and volume and sum of TM occupancy (g_{total}) for the sample calcined in N_2 were larger than those for the sample calcined in air. The elemental analysis data showed that nominal Fe:Ni:Mn ratio was kept after preparation and the Li/(Fe+Ni+Mn) ratio for the sample calcined in N_2 was smaller than that for the sample calcined in air. These results mean that at least one of TM ions in sample calcined in N_2 was reduced. Fe valence state was checked by ^{57}Fe Mössbauer spectroscopy for the sample with y=0.15. The area fraction of minor $Fe^{3.5+}$ or Fe^{4+} component for the sample calcined in N_2 was smaller than that for the sample calcined in air. Therefore, Fe valence state is responsible for the calcination atmosphere.

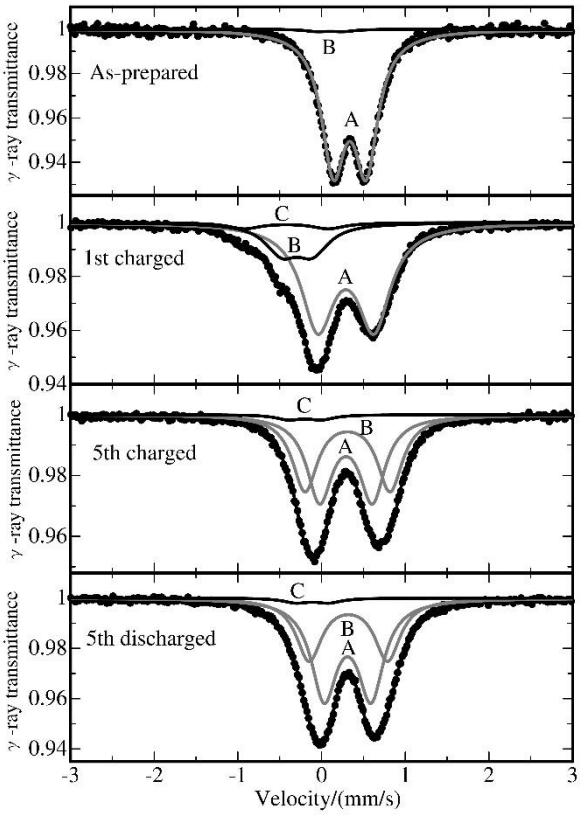

Fig. 1 ^{57}Fe Mössbauer spectra for $Li_{1+x}(Fe_{0.15}Ni_{0.15}Mn_{0.7})_{1-x}O_2$ ($0<x<1/3$) calcined in N_2. Gray symmetric doublet corresponds to high-spin trivalent iron.

Fig. 1 depicts change in Fe valence state during different charge and discharge depths for $Li_{1+x}(Fe_{0.15}Ni_{0.15}Mn_{0.7})_{1-x}O_2$ ($0<x<1/3$) calcined in N_2 atmosphere. On 1st charging, pentavalent Fe components (B and C) [2] were observed with trivalent one (A), indicating that Fe^{3+} to Fe^{5+} oxidation behavior was detected. The area fraction of pentavalent Fe component is drastically reduced at the end of charging (5th charging), meaning that most Fe ion is trivalent state. Almost same spectrum was obtained at 5th discharged state. The results show that the trivalent iron was utilized on initial Li-extraction process. Therefore, suppress of pentavalent iron reduction until the end of charging is necessary to improve its electrochemical performance.

REFERENCES:

[1] M. Tabuchi *et al.*, J. Power Sources, **196** (2011) 3611-3622.
[2] G. Demazeau *et al.*, Mat. Res. Bull, **16** (1981) 1465-1472.

CO4-26 Evaluation of Structural Vacancies for Semiconducting Quasicrystal Approximant Al-Si-Ru by Positron Annihilation Spectroscopy

K. Kitahara[1], K. Kimura[1], A. Kinomura[2], Q. Xu[2],
N. Oshima[3], Y. Ohota[4], I. Kanazawa[4]

[1]*Department of Advanced Materials Science,The University of Tokyo*

[2]*KURNS*

[3]*National Institute of Advanced Industrial Science and Technology*

[4]*Department of Physics,Tokyo Gakugei University*

INTRODUCTION: One interesting feature of many exotic physical properties of Al-based quasicrystals is tendency to show high electrical resistivities and negative temperature coeffcients[1]. The physical origin of these anomalous properties has not been satisfactorily explained so far. Semiconducting quasicrystals have attracted attention, not only from the perspective of the academic field , but also from the standpoint of application to thermoelectric materials to realize a direct conversion between the thermal and electrical energies. Kimura et al.[2] have shown that the vacant centers of the Al-based icosahedral clusters plays an important role for stabilities and chemical bonding nature of clusters. The various experimental results[3-5] support that the structural vacancy of the icosahedral clusters plays an important role in the bonding nature and electronic transport properties in Al-based qujasicrystals and approximants. Recently Kimura and coworkers[6] have discovered the semiconducting-like quasicrystal approximant of Al-Si-Ru. It is of significance to study the semiconducting Al-Si-Ru quasicrystal approximant from the standpoint of structural vacancies. Positron annihilation method is powerful one for detecting structural vacancies of icosahedral quasicrystals[7]. In this study, we have estimated structural vacancies of the semiconducting qusicrystal approximant of Al-Si-Ru by means of positron annihilation methods.

EXPERIMENTS :
Bulk samples of 1/0-Al-Si-Ru and χ phase Al-Si-Ru were sealed in a quarts tube and annealed for 1 week at 1000 C and annealed for 1 week at 927 C,respectively. The phase characterization was performed by X-ray diffraction. The Doppler broadening spectra were measured using a slow variable mono-energetic positron beam. CDB measurements were performed with a collinear setup of two Ge detectors.

RESULTS and DISCUSSIONS:
Figure 1 shows X-ray diffraction patterns of C-phase $Al_{69}Si_{17.5}Ru_{23.5}$(from up,C0,C2,C5,C9) and a diffraction pattern of the model of approximate 1/0 Al-Si-Ru(down). By using the slow positron beam, we have estimated the change in S-parameter with positron-incident energies in C-phase $Al_{69}Si_{17.5}Ru_{23.5}$(semiconduction approximate) and χ phase $Al_{66}Si_{15}Ru_{19}$. In both materials, S-parameter increases remarkably from ~0 to~1 keV. This means that density of structural vacancies of C-phase Al-Si-Ru is comparable with that of χ phase Al-Si-Ru. Comparing with other experiment results[5,8], densities of structural vacancies of C-phase Al-Si-Ru and χ phase Al-Si-Ru are comparable with those of $1/1Al_{73}Re_{17}Si_{10}$ [5] and 1/0 AlPdRu[8]. Taking account of the previous studies[5,9], densities of structural vacancies of C-phase Al-Si-Ru and χ phase Al-Si-Ru are estimated to be order of 10^{20} cm^{-3}. Then we have done the coincidence Doppler broadening(CDB) spectra of C-phase Al-Si-Ru and χ phase Al-Si-Ru.

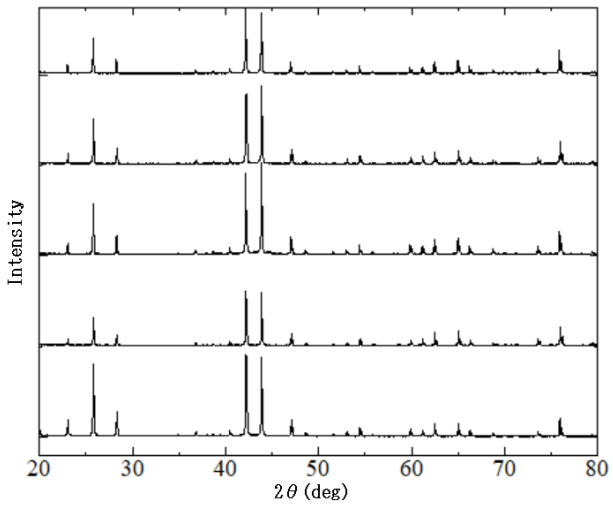

Figure 1: X-ray diffraction patterns of C-phase $Al_{69}Si_{7.5}Ru_{23.5}$ and the model of 1/0 Al-Si-Ru(from up to down).

Experimental results suggested strongly that the trapping sites of C-phase and χ phase seem to be similar. The present study shows that there exist deformed Mackay clusters[10] with vacant centers in semiconducting C-phase Al-Si-Ru.

REFERENCES:
[1] K. Kimura and S. Takeuchi,in Quasicrystals:The State of Art,2nd ed.,D.P. Divincenzo and P.J. Steinhart,eds.,World Scientific, Singapore,1999.pp.325-309.
[2] K.Kimura *et al.*,J.Solid State Chem.133(1997)302.
[3] K.Sato *et al.*,Phys.Rev.B59(1999)6712.
[4] K.Kirihara *et al.*,Phys.Rev.Lett.85(2000)3468.
[5] K.Yamada *et al.*,Phil.Mag.98(2018)107.
[6] Y.Iwasaki *et al.*,Phys.Rev.Mater.3(2019)61601.
[7] I.Kanazawa *et al.*,Phys.Rev.Lett.79(1997)2269.
[8] M.Nakajima *et al.* in preparing.
[9] K.Sato *et al.*,Appl.Surf.Sci.194(2002)155.
[10] R.Simura *et al.*,Mater.Trans.58(2017)1101.

CO4-27 Effect of gamma radiation on ultra-micro structure of hardwood cell-wall

K. Murata, Y. Imataki, M. Nakamura, T. Saito[1]

Graduate School of Agriculture, Kyoto University
[1]Institute for Integrated Radiation and Nuclear Science, Kyoto University

INTRODUCTION: Space-wood project (LignoStella project) is performed by Kyoto University collaborating with Sumitomo forestry Co Ltd in order to challenge to use wood-material in outer space. Firstly, possibility to use wood material in outer space has to be confirmed because a small wooden artificial satellite is going to launch until 2023. Space exposure test of wood specimen started on ExBAS at ISS in March 4, 2020. The wood specimen is going to be exposed until Dec. 2020. They will be affected by atomic oxygen and cosmic ray. In this study, effect of gamma-ray irradiation on cell-wall of wood material was studied on the ground in parallel with the exposure tests in outer space.

EXPERIMENTS: The sample was Honoki (*Magnolia obovate*), which is 100 mm (length) ×10 mm (radial) × 2 mm (tangential) in size. They were conditioned in 20 °C and 60%RH for a few weeks before the dose test. They were irradiated for 5 hours, and four types of dose was performed, which is 30 kGy, 3 kGy, 1kGy and 0.1 kGy. Before and after irradiation, bending test was performed to obtain Young's modulus in 3 point bending test until 5 N. After irradiation, ultra-micro structure of cell wall was observed using a small angle X-ray scattering analysis (SAXS) (Rigaku, Nano-viewer). The camera distance was 1000 mm and X-ray scattering (wave length 0.154 nm) was recorded by 2-dimensional detector (PILATUS 100K). Diameters of particle or pore and fractal dimension, distance between crystals were measured using scattering profiles.

RESULTS: As shown in Fig. 1, density of wood specimen of 30 kGy dose decreased by approximately 1 kg/m^3 more than other dose specimens. Young's modulus of wood specimen of 30 kGy dose changed by gamma irradiation, but other specimen did not change even if density decreased. As shown in Fig. 2, fractal dimensions did not change by irradiation. We think that mass fractal dimension show density of electron in cell-wall matrix, and meso-pore in cell-wall may not change by irradiation. As shown in Fig. 3, diameters of particle or pore were obtained using Guinier plot. The size was similar to diameter of cellulose micro fibril (CMF), so we determine that the particle is CMF. Diameters of CMF decreased slightly by irradiation. As shown in Fig. 4, distances of CMF were obtained using Krathy plot. The change in distance was similar to that of the diameter. But, we can not understand why Young's modulus and density of 30 kGy decreased more than other species.

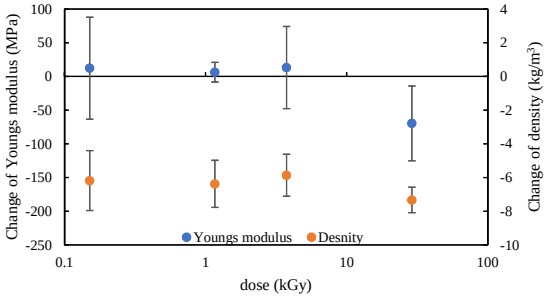

Fig. 1. Change of specific Young's modulus and density by gamma irradiation.

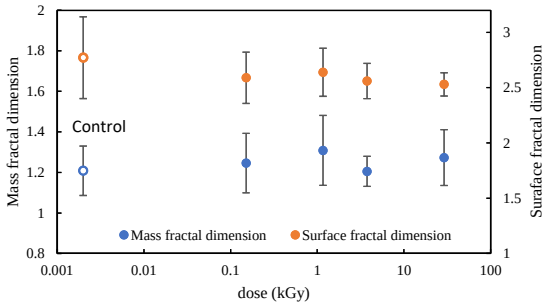

Fig. 2. Change of fractal dimension by gamma irradiation.

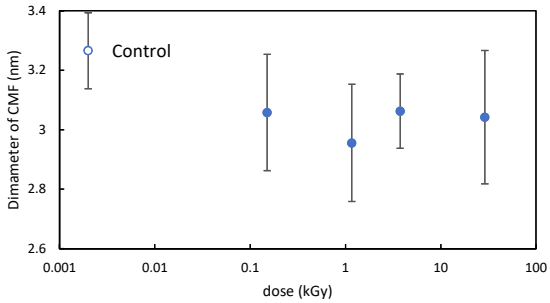

Fig. 3. Change of diameter of CMF by gamma irradiation.

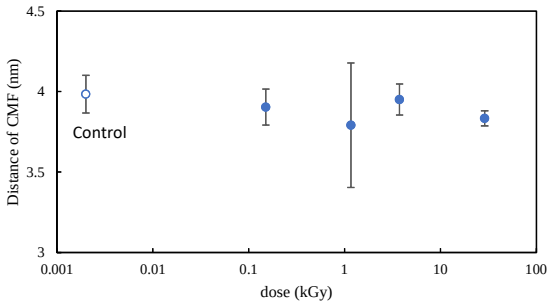

Fig. 4. Change of distance of CMF by gamma irradiation.